THE EMISSION SPECTRUM OF THE CARBON MONOCHLORIDE MOLECULE

THE EMISSION SPECTRUM OF THE CARBON MONOCHLORIDE MOLECULE

by

ROBERT DIXON GORDON, B.Sc.

A Thesis

Submitted to the Faculty of Graduate Studies

in Partial Fulfillment of the Requirements

for the Degree

Master of Science

McMaster University

May 1961

MASTER OF SCIENCE (1961)
(Chemistry)

McMASTER UNIVERSITY
Hamilton, Ontario

TITLE: The Emission Spectrum of the Carbon Monochloride Molecule.

AUTHOR: Robert Dixon Gordon, B. Sc. (McMaster University)

SUPERVISOR: Dr. G. W. King

NUMBER OF PAGES: vii, 103

SCOPE AND CONTENTS:

A search was made for the emission spectra of any free radicals which might be excited in a discharge through halogenated methanes. A band system in the 2000 A° region was photographed under high resolution, and assigned to a $^2\Delta_{inv}$ case (b) - $^2\Pi_{reg}$ case (a) transition in the CCl molecule. Rotational and vibrational analyses of this spectrum were performed. These analyses have also been reported elsewhere.[61]

ACKNOWLEDGMENTS

I sincerely wish to thank Dr. G. M. King for his help and encouragement in directing this research.

I am grateful for many profitable discussions with my colleagues Messrs. J. L. Hencher, V. A. Job, G. L. Nalli, and D. C. Moule.

I am indebted to Imperial Oil, Limited for the award of an Imperial Oil Graduate Research Fellowship during the period 1959 - 1960 in which this research was done.

Finally, I would like to thank my wife, Diane, for her help in typing this thesis.

TABLE OF CONTENTS

CHAPTER 1 Page

Introduction 1

CHAPTER 2

Experimental Techniques Useful in the Production of Free Radical Spectra 4

CHAPTER 3

Exploratory Experimental Work: A Search for the Emission Spectra of Free Radicals Excited in a Discharge through Halogenated Methanes 12

CHAPTER 4

Observed Spectra and Discussion 20

CHAPTER 5

Analysis of the CCl Emission Spectrum: Introduction and Historical Review 35

CHAPTER 6

Production and Measurement of the Emission Spectrum of CCl Under High Resolution 38

CHAPTER 7

Rotational Energy Levels and Spectra of Diatomic Molecules in Doublet States 42

I. Rotational Energy Levels in Hund's Cases (a) and (b) 42

II. Spin Doubling in Case (b) States 50

III. Λ-type Doubling 50

CHAPTER 7, continued — Page

IV. Selection Rules and Allowed Transitions . . . 53

CHAPTER 8

Rotational Analysis of the 2780 A° Band of the CCl Molecule 60

I. Assignment of the Transition 60

II. The Combination Principle 63

III. Lower State Constants and Numbering of the Lines 64

IV. Upper State Constants. 68

V. Origins of the Sub-bands 69

VI. Summary of Measured Quantities for the 2780 A° Band 71

VII. Fine Structure 71

CHAPTER 9

Vibrational Analysis of the CCl Spectrum 76

CHAPTER 10

Discussion of Results of the CCl Analyses 86

APPENDICES

I. Derivation of Rotational Energy Expressions from the General Hill and Van Vleck Expression 89

II. Formulae for the Frequencies of the Lines in a $^2\Delta$ case (b) - $^2\Pi_{reg}$ case (a) Transition . .93

III. Frequencies and Rotational Assignments of the Observed Lines in the 2780 A° Band of CCl 97

BIBLIOGRAPHY 101

LIST OF TABLES

		Page
Table 1.	Wavelengths and Intensities of the CF_2 Band Heads.	23
Table 2.	Impurity Spectra Observed in Discharges in Freons.	27
Table 3.	Observed Atomic Lines of Helium.	28
Table 4.	Impurity Spectra Observed at High Partial Pressures of Helium.	29
Table 5.	Results Obtained from Equations (10) and (11) with various Numbering Schemes.	66
Table 6.	Rotational Constants for the (0-0) Band of CCl . .	70
Table 7.	Frequencies and Assignments of Band Heads and Bands.	80
Table 8.	Measured Vibrational Constants for CCl.	85
Table 9.	Formulae for the Branches of a $^2\Delta$ Case (b) - $^2\Pi$ Case (a) Transition.	94
Table 10.	Vacuum Wavenumbers and Rotational Assignments for the 2780 A° Band of CCl.	98

LIST OF FIGURES

		Page
Figure 1.	The Schuler Tube.	8
Figure 2.	Vacuum System.	19
Figure 3.	CCl Emission Bands and Associated Continua. . . .	22
Figure 4.	CF_2 Emission Bands and Impurity Spectra, 2400 - 3200 A°.	25
Figure 5.	Impurity Spectra, 3700 - 5700 A°.	30
Figure 6.	Impurity Spectra in Pure Helium	31

Figure 7. High-resolution Spectrograms of the CCl Spectrum at 2780 and 2850 A°. 41

Figure 8. The Diatomic Molecule as a Symmetric Top. 44

Figure 9. Coupling in Hund's Case (a).. 44

Figure 10. Coupling in Hund's Case (b). 44

Figure 11. Correlation between Cases (a) and (b). 49

Figure 12. Coupling in Hund's Case (d) 52

Figure 13. Correlation between Cases (b) and (d) for L= 1. 52

Figure 14. Λ-type Doubling in Q_1 and R_1 Lines. 54

Figure 15. The J" = 3.5 Lines of the Twelve Branches of a $^2\Delta$ (b) - $^2\pi_{reg}$ (a) Transition.. 56

Figure 16. Fortrat Diagrams. 59

Figure 17. A Microdensitometer Trace of the CCl Spectrum at 2780 A°under High Resolution. 62

Figure 18. Fine Structure 73

Figure 19. Microdensitometer Traces of the CCl Spectrum at 2714, 2780, 2850, and 2920 A°. 78

Figure 20. A High-resolution Microdensitometer Trace of the CCl Band Heads at 2850 A°. 79

CHAPTER 1.

INTRODUCTION

Spectroscopic studies have played a most important part in the investigation of molecular structure. In the study of the short-lived species commonly called free radicals*, spectroscopic techniques are perhaps especially valuable due to the limited applicability of more conventional chemical methods. In the first place, spectroscopic investigation is a sensitive means of confirming the existence of radicals whose presence might be expected on other grounds, although, of course, the failure to detect a radical by its spectrum does not preclude its existence. Electronic spectra provide information on the energy and symmetry of radicals, and in the case of simpler molecules, vibrational and rotational constants may be obtained with considerable accuracy. If this latter information is sufficiently complete, it is possible to calculate the thermodynamic properties of the radical. The rotational constants can be used to derive bond angles and distances which are useful in testing the predictions of quantum chemistry.

*Following the example of Ramsay[1] in his review of free radical spectroscopy, a free radical will be defined as a short-lived molecular species, whether or not it has an unpaired electron.

Although the spectra of several hundred diatomic free radicals have been observed, comparatively few polyatomic radicals have been studied successfully. This is largely due to the difficulty encountered in providing a means of excitation energetic enough to decompose the parent substance, yet gentle enough not to disrupt it into ions or into atomic or diatomic molecular fragments.

Recently, Venkateswarlu[2] and Johannin-Gilles[3] observed the emission spectrum of the CF_2 radical in a discharge through fluorinated methanes. Laird, Andrews, and Barrow[4] obtained many of the same bands in absorption under similar conditions. Although this molecule has yet to be studied under high resolution, it was the first polyatomic radical to be identified positively by an analysis of its spectrum.[5] Venkateswarlu's partial analysis, performed under low resolution, indicated that the radical is bent, with different bond angles in ground and excited states. Walsh[6] has made interesting theoretical predictions about triatomic molecules of this type, relating the bond angle to the number of electrons. A high resolution study of the CF_2 spectrum, including a precise determination of the bond angle, would therefore be particularly significant.

Accordingly, experimental work was undertaken in an attempt to rephotograph the CF_2 spectrum under high resolution, as well as to search for "mixed" radicals of the type CHF,CFCl, etc., there being no apparent reason why their spectra should not be equally accessible. This work is described in Chapters 2,3, and 4 of this thesis.

Unfortunately, no spectra due to such "mixed" radicals were observed. The CF_2 spectrum was observed in emission under low resolution, as in previous work.[2-4] A band system of the CCl radical, however, was observed in emission and photographed under high resolution. Rotational and vibrational analyses were performed. The study of this spectrum constitutes the major part of the work described in this thesis, and is dealt with in Chapters 5-10.

CHAPTER 2.

EXPERIMENTAL TECHNIQUES USEFUL IN THE PRODUCTION OF FREE RADICAL SPECTRA

The spectra of polyatomic free radicals have been discussed extensively in recent articles by Herzberg[5] and by Ramsay.[1] This chapter is devoted to a brief account of the methods that have been used to produce free radical spectra. As only two species, OH and CS, have been examined in the gas phase in the infrared or microwave region, this account is limited to electronic spectra. Most of the work on polyatomic species has been done since 1950.

Probably the most useful technique for obtaining polyatomic free radical spectra has been flash photolysis, as developed by Norrish and Porter[7], by Herzberg and Ramsay[8], and by Davidson and co-workers.[9] A very high concentration of radicals is produced for a short time by the photodissociation of a suitable gas with an extremely intense flash of light. This flash is produced, for a duration of several microseconds, by discharging a bank of condensers through specially designed lamps. Immediately afterwards, a similar lamp is flashed to provide the source continuum needed to observe absorption spectra. A set of multiple reflection mirrors, as described by White[10], is often used to increase the effective

absorption path length. These are concave mirrors, placed at either end of the reaction vessel in such a way that the light traverses the vessel as many as twenty times. The absorption spectra of a number of polyatomic radicals, including NH_2, PH_2, HCO, CH_3, HS_2, NCO, NCS, and CH_2, have been obtained by this technique.

When the intense excitation conditions of flash photolysis are not necessary, continuous photolysis with a lower intensity of exciting light has been used to produce radicals, whose spectra may be obtained in absorption or fluorescence. Flame sources have been used for emission spectra. For example, the "α-bands of ammonia" were observed long ago in ammonia-oxygen flames. More recent high resolution studies, using flash photolysis, indicated that the emitter of these bands is the NH_2 radical.

Purely thermal excitation has also been used. Margrave and Wieland[11] found the absorption bands of CF_2 when they decomposed CF_4 in a carbon furnace at 1900° K. The radicals C_3 and SiC_2 have also been observed with this technique. Shock waves have been used to produce very high temperatures in gas mixtures, but only diatomic radical spectra have been obtained in this way.

The spectra of free radicals in the solid state have also been investigated. Radicals may either be produced in the gas phase and then rapidly frozen, or produced in the solid state itself by some form of irradiation. A number of aromatic radicals have been produced in frozen ether-pentane-alcohol glasses and their spectra investigated. Large organic radicals can be prepared by conventional chemical means,

and are stable in solution. For example, hexaphenylethane in ether solution gives rise to the triphenylmethyl radical, but in liquid sulphur dioxide solution produces the triphenylmethyl cation. The spectra of these substances have been investigated in solution.

Although they have not been as useful as flash photolysis in the production of polyatomic radical spectra, discharge tubes have played a most important role in free radical spectroscopy in general. As discharge tubes were used in the work described in this thesis, and since most previous work on the CF_2 spectrum involved gaseous discharges, this means of excitation will be described in greater detail.

The uncondensed electric discharge between electrodes in a gas at low pressure is frequently used. It is operated at a potential of 5,000 to 15,000 volts and a current of one to ten milliamperes. The power is supplied by a suitable transformer operating off the A.C. supply mains. The behaviour of such a low frequency discharge is similar to that of a D.C. discharge in that the electrons actually pass from one electrode to the other. Positive ions produced by the collision of electrons and gas molecules are swept to the cathode where their impact causes the emission of more electrons, thus sustaining the discharge. Because of their relatively low mobility, as compared to electrons, these ions build up a large space charge. As a result, the potential drop occurs in a small region near the cathode. Throughout the major portion of the tube the potential gradient is lower. The uniform visible glow excited in this region is called the positive column.[12]

The particular type of discharge tube used in this work was designed by Schuler[13] to excite the spectra of larger organic radicals without breaking them into small fragments. It is illustrated in Fig. 1. It differs from ordinary electric discharge tubes only in that the gas being studied is frozen out in the liquid nitrogen traps (C) before reaching the electrodes. This feature is intended to isolate the gas from the very high energy electrons in the immediate vicinity of the cathode which would be likely to dissociate the gas into atomic or diatomic fragments. An inert carrier gas, such as helium, which remains gaseous at liquid nitrogen temperatures, is added to the streaming organic gas to provide electric conduction between the traps and the electrodes.

This type of discharge is a fruitful means of exciting new spectra, especially those due to large radicals. For example, Schuler found that a certain spectrum was emitted by the excitation of about twenty different parent gases, including benzene, hexane, and acetylene. Callomon[14] was able to show that its emitter was the diacetylene ion $C_4H_2^+$.

Discharges excited by microwave or other high frequency radiation have also proved useful. The essential difference between such a high frequency discharge and a low one is that the period of oscillation of the exciting field is too short to allow the electrons to flow between electrodes before the direction of the field is reversed. The electrons merely oscillate in the gas with an amplitude less than the dimensions of the discharge tube.[15] Since the chief limitation to the drift velocity of the electrons is collision with gas molecules, the transition from low to high frequency behaviour occurs when the

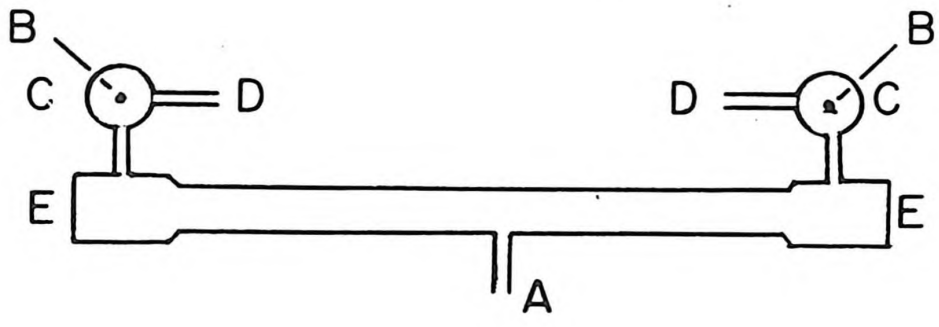

Fig. 1. The Schuler Tube: A, gas inlet; B, hollow aluminum electrodes; C, liquid nitrogen traps; D, gas outlets; E, quartz windows.

frequency of the exciting field exceeds the frequency of electron-molecule collisions.

In a high frequency discharge the velocity of the electrons is 90° out of phase with the accelerating field. That is, reversals in the direction of motion of the electrons lag behind the corresponding reversals of the field, with a delay equal to one quarter of the period of oscillation of the latter. The kinetic energy gained by the electrons is thus returned to potential energy in the field when the latter is reversed. The electrons absorb no net power. If, however, the electron collides elastically with a molecule, it is deflected from its path, and its motion becomes partly random. The random component of its kinetic energy is not returned to the electric field, and net power absorption results.* In this way the electrons gradually gain sufficient energy to take part in inelastic collisions, exciting or ionizing the molecules they strike.

McCarthy[16] has described the advantages of a microwave discharge, as opposed to a low frequency discharge, in the production of radicals. He stated that the yield of radicals per unit energy input is about ten times greater with high frequency than with low frequency excitation. This is perhaps due to the fact that in an ordinary electric discharge, a good deal of energy is lost as heat when the positive ions bombard the cathode, while in a microwave discharge, all the absorbed energy is used in the excitation or thermal agitation of the gas. He also stated that emission spectra from a microwave glow

*In an elastic collision, the electron loses only a negligible fraction of its kinetic energy, about 2 x (mass, electron)/(mass, molecule), to the molecule with which it collides, retaining the rest.

show more extensive banded structure than the corresponding spectra from a low frequency discharge. Several pieces of evidence were put forward for a microwave discharge being a more efficient producer of radicals.

When air was excited in a microwave discharge, nitric oxide was produced. Under certain conditions, the effluent stream from a discharge in flowing air gave off a faint yellow light for 30 cm. downstream from the discharge zone. As the luminous particles were not deflected towards the tube walls by powerful electric or magnetic fields, they could not be ionic. These observations were duplicated in the work described in this thesis. Furthermore, McCarthy found that when methane was passed through the discharge, and the products were allowed to strike a liquid-nitrogen-cooled wall, significant quantities of ethane and ethylene were formed.

Finally, something should be said about the relative merits of absorption and emission spectroscopy in free radical studies. Absorption has several advantages. One concerns the identification of the molecule giving rise to an observed spectrum. If on chemical grounds one would expect a certain molecule to be present in high concentration, it is quite probable that it will give rise to any absorption spectra observed. In emission, however, the emitter of the observed spectrum is not necessarily one of the major chemical species that might be expected to be present. This is illustrated by the fact that a large number of unrelated organic gases, when excited in a Schuler tube, all produced the emission spectrum of the diacetylene ion.

The presence of a band system in absorption identifies the lower state of the transition as the ground state. On the other hand, one is

likely to observe additional transitions in emission which do not involve the ground state. The intensity distribution and its temperature dependence in an absorption spectrum are useful aids in the assignment of vibrational bands, but this is not usually so in emission.

The chief disadvantage of absorption is that it requires a large concentration of radicals in the ground state, which is difficult to produce except by flash photolysis. It is true that Barrow[4] observed the CF_2 spectrum in absorption, using a high frequency discharge through fluorinated hydrocarbons; however, both he and Simons and Yarwood[17] found that this molecule has an unusually long ground state lifetime, of the order of one second, under the conditions of the experiment. Even so, a large bulb had to be used to inhibit the wall-catalyzed recombination of the radicals. A large stationary concentration of radicals is not necessary in emission.

Another disadvantage of absorption is of particular importance in exploratory work such as is described in this thesis. While spectral lines in emission are reasonably broad due to the Doppler effect, they can be very narrow in absorption at room temperature. Herzberg[5] pointed out, in connection with absorption studies of NH_2, that its spectral lines, which are widely spaced, are so narrow that they would not be detected at all except with quite high resolution. However, it is very inconvenient to use high resolution instruments in preliminary exploratory work as a great many plates must be taken to observe the entire spectral region.

CHAPTER 3.

EXPLORATORY EXPERIMENTAL WORK: A SEARCH FOR THE EMISSION SPECTRA OF FREE RADICALS EXCITED IN A DISCHARGE THROUGH HALOGENATED METHANES.

In searching for the spectrum of CF_2, and that of any "mixed" radicals, it was decided to follow the lead of Venkateswarlu[2] and Johannin-Gilles[3] and to study the emission spectra excited by a discharge in halogenated methanes. In addition to CF_4 and CCl_2F_2 which these workers employed, CCl_4, CCl_3F, $CHCl_2F$, CHF_3, and $CBrF_3$ were used in the work described in this chapter. Both the Schuler-type discharge tube and a microwave discharge were used. On the basis of the arguments in the last chapter, emission rather than absorption techniques were employed.

It may be that better results could have been obtained by using other parent compounds. Although Barrow[4] merely reported having used "fluorocarbon" in his work on CF_2, Dyne[18] has stated, on the basis of a private communication from Barrow, that this substance had a carbon: fluorine ratio of 7:12 and contained many CF_2 groups. Douglas[19] observed CF_2 in the flash photolysis of fully fluorinated acetone. The methylene radical, CH_2, was first observed spectroscopically in the flash photolysis of diazomethane (CH_2N_2).[20] Previous attempts to produce it from ketene (CH_2CO) failed, although CO bands appeared with considerable intensity.[5] The SiF_2 spectrum, however, was observed in

a discharge through SiF_4.[21] The search for radical spectra described in this thesis was confined to the use of halogenated methanes as parent substances.

Except for carbon tetrachloride, which was of reagent grade quality, all the halogenated methanes were gases at room temperature, and were supplied by the Mathieson Company in lecture bottles. These halogenated methanes are commonly called Freons.

The Schuler tube was identical to the one illustrated in Fig. 1. It was 1.4 m. long and 7 cm. in diameter. In order to make use of all the light emitted in such a large tube, a single lens was employed to match the optical apertures of the tube and the spectrograph. Multiple reflection mirrors, as described in Chapter 2, were also used.

The microwave discharge tube was constructed from 12mm. glass tubing and fitted with quartz windows. Exciting radiation was supplied by a Raytheon "Microtherm" microwave generator, model CMD_4, delivering 100 watts power at 2450 megacycles per second. The half-wave antenna, with a cylindrical parabolic reflector to focus radiation on the tube, was mounted 1 cm. from the outside of the tube. The visible glow, quite localised, was only about 5 cm. long. Despite the fact that radicals are lost at the tube walls, a relatively narrow tube had to be used, as the microwave generator could not support a discharge in a large bulb. Barrow[4] was able to excite spectra in a large bulb containing gas at low pressure, but he used a radio frequency source (1 megacycle per second).

The vacuum system used with both discharge tubes is illustrated in Fig. 2. The Freons were admitted at (A), and resublimed at least three times between the U-tubes (B), (C), and (D), and stored in

the bulbs (F). Helium, when used as an inert carrier, was purified by flowing through the charcoal trap (H) which was cooled to liquid nitrogen temperatures.

Gases were flowed continuously through the discharge tube, and frozen out in the cold trap (G) before reaching the pump. The partial pressures of gases in the tube were controlled by means of the needle valves (N_1) and (N_2). The pressures at various points in the system were measured by Pirani gauges (D). The discharge tubes were viewed end-on by the spectrograph.

Spectra obtained in this preliminary work were photographed under low resolution on a Bausch and Lomb 1.5 m. grating spectrograph, model 11, with a resolving power of 70,000 and a dispersion of 15 A°/mm. in the first order. With Ilford HPS or Kodak 103a0 35 mm. film, exposure times were of the order of five minutes with a microwave discharge, and thirty minutes with the Schuler tube.

The design of the spectrograph was such that the regions 7400 - 3700 A° and 3700 - 1850 A° were obtained in the first and second orders respectively on the same length of film. The overlapping first and second order spectra could be separated to a large extent by inserting 2 mm. thicknesses of Chance Brothers' glass filters OY10 and OX7 in front of the spectrograph slit. These filters transmitted the regions 3600-25,000 A° and 2400 - 4100 A° respectively. With these filters it was possible to record separately the overlapping orders in the range 2400 - 6500 A° . The upper wavelength limit was set by the sensitivity of the film. The region from 2400 A° to the onset of the vacuum ultraviolet at about 1900 A° , however, was absorbed by both filters, and it was impossible to work

without a filter because of intense impurity spectra in the overlapping first order region. Bromine gas and cobalt or nickel sulphate solutions absorb more strongly between 3800 and 4800 A° than they do between 1900 and 2400 A° .[22] The difference in extinction coefficient, however, was too small to permit the use of these materials as filters.

Preliminary studies were therefore restricted to the spectral region of 2400 - 6500 A° , and the possibility remains that interesting spectra could be found at lower wavelengths. Two band systems of CF, for example, have been observed between 1977 and 2240 A° ,[23] as well as a system thought to be due to CCl^+[25,26] in the region 2367 - 2434 A° . Further studies, from 2400 A° to the onset of the vacuum ultraviolet, might be facilitated by using an external predispersion apparatus to eliminate the overlapping first order spectrum.

A considerable amount of deposit formed on the walls of the microwave discharge tube, and it created a serious problem in that its surface was very effective in removing free radicals. As more deposit formed, the intensity of emission of radical spectra decreased, and after about twenty hours' use, the discharge tube had to be replaced. The deposit also formed on the Schuler tube walls, but here, with a much larger tube and a less localized discharge, it was less troublesome. Two types of deposit formed, one a thin white film, and the other a tarry brown substance. The latter outgassed strongly when heated, giving a scaly, black product, much like graphite. The volatile products of the discharge, which were frozen out in the cold trap, included unused starting material and the appropriate halogens.

Chlorine was identified by its odour, and bromine by its reddish colour which disappeared upon the addition of styrene. Fluorine probably was formed as well, but, since it boils at -188° C, it would not be frozen out at liquid nitrogen temperatures.

Throughout the work, two main objects were kept in mind. They were to reduce the intensity of emission due to impurities, and to vary the conditions of the discharge in such a way as might favour the formation of interesting radicals. Not only were the impurity spectra likely to obscure any weaker radical spectra, but also, if excited preferentially in competitive reactions, the impurities might prevent the excitation of other radicals. The impurity spectra were never completely eliminated, but they were kept low in intensity, and did not occur in the same regions as the spectra of the CCl and CF_2 radicals which were observed.

In general, better results were obtained with the microwave discharge. With it the impurity spectra were weaker, and the CF_2 bands stronger. It was also possible to excite the CCl spectrum, which was not observed with the Schuler tube. These differences were more likely due to improved experimental techniques used in the microwave work rather than to the different nature of the discharge. Other workers[24, 27-31] were successful in obtaining the CCl emission spectrum by using low frequency electric discharges.

It was found that the same radical spectra were excited whether or not a helium carrier gas was used, although there were differences in the spectra of impurities. It proved convenient to use a carrier, as there was then less tendency for the discharge to be extinguished. For example, with pure CF_4 and no carrier, the CF_2 bands did not

become prominent unless the pressure was greater than 0.1 mm., but it was very difficult to maintain the discharge at such a high pressure of the Freon. The large concentration of CF_4 led to excessive formation of deposit on the walls as well, and to excessive consumption of the Freon. The same spectrum could be obtained more conveniently with helium at 0.1 and CF_4 at 0.05 mm. partial pressures.

The intensity of impurity spectra was reduced by flaming the walls of the discharge tube to drive off adsorbed gases. It was thought that impurities were being released from the tube walls by the heat generated by absorption of the microwave radiation. The tube was cooled in dry ice, but with no improvement. It has been mentioned how the Freons were purified by resublimation under vacuum. In order to check the efficiency of this process, CCl_2F_2, purified in the same manner, was analyzed gas chromatographically. Atmospheric impurities were present in less than 0.1% concentration. This ruled out the possibility of the formation of an azeotrope between Freon and air which might lessen the effectiveness of the sublimations.

The pressure in the discharge tube was varied extensively, as was the helium : Freon ratio. A discharge could be maintained at total pressures as low as three microns, but only impurity spectra were emitted. The intensity of radical spectra increased with increasing pressure of the Freons. The highest pressure at which a discharge could be maintained varied from 0.1 to 5 mm. for the various gases.

The exciting power was also varied. The Schuler tube was operated at from 3640 to 7300 volts, and from two to five milliamperes. At higher power levels, the electrodes became hot enought to crack the

surrounding glass. The microwave power output had to be limited to 80 watts to prevent the heat absorbed by the glass from puncturing the tube walls. The only observed result of increasing the power levels within these limits was an increase in the intensity of emission.

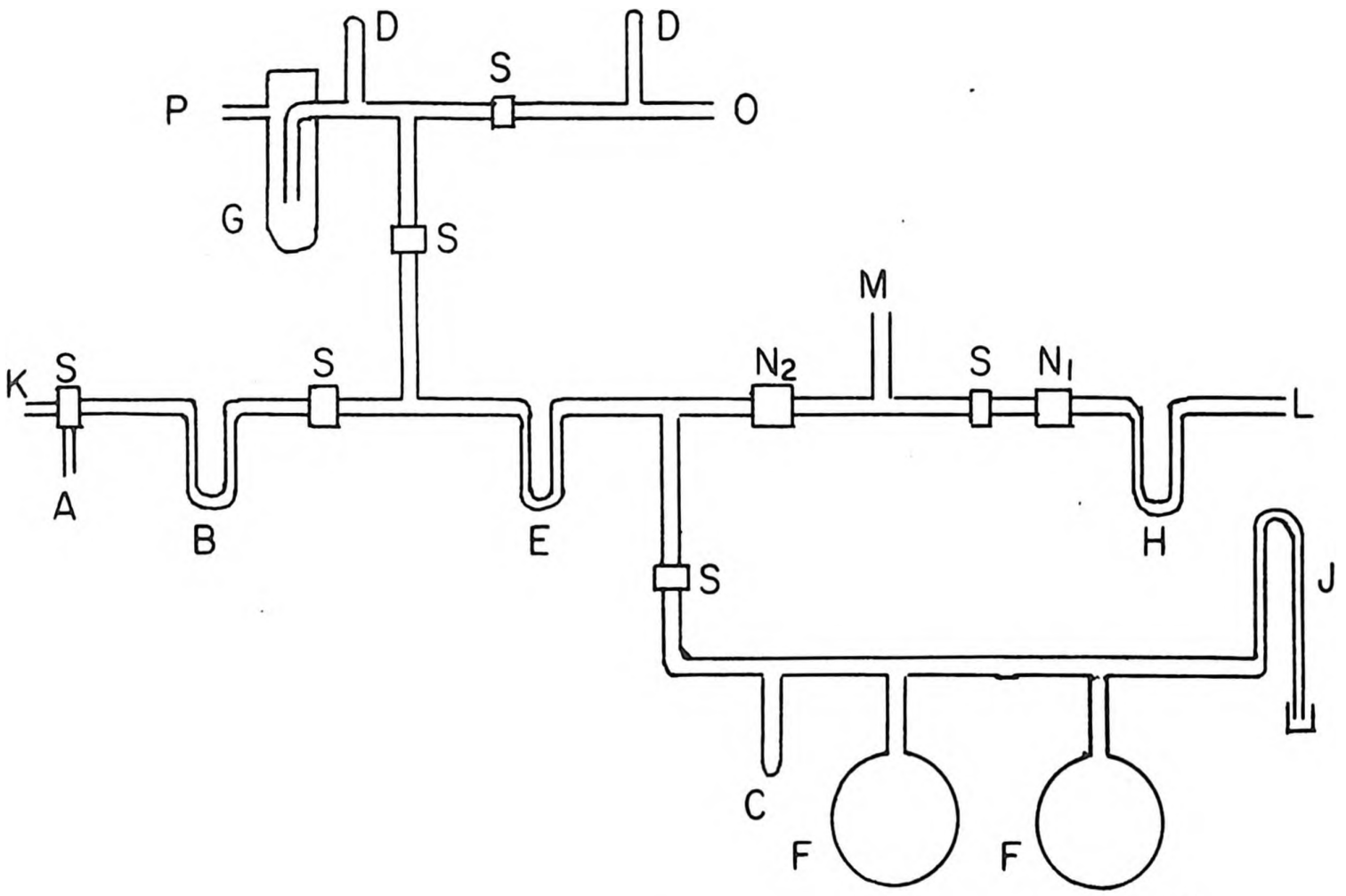

Fig. 2. Vacuum System: A, Freon inlet; B,C,E, U-tubes; D, Pirani gauge heads; F, storage bulbs; G, cold trap; H, charcoal trap; J, manometer; K, vent; L, helium inlet; M, to discharge tube: N_1,N_2, needle valves; O, from discharge tube; P, to diffusion pump.

CHAPTER 4.

OBSERVED SPECTRA AND DISCUSSION

The emission spectra observed in the preliminary experiments are summarized below. The same free radical spectra were obtained whether or not helium was used as a carrier gas, but different impurity spectra appeared at high ratios of helium to Freon. With the exception of the results described in section (f), obtained when $CBrF_3$ was excited in a low frequency discharge, all the spectra described below were obtained by microwave excitation.

(a) Four clusters of double-headed, violet-degraded bands, at 2714, 2760, 2850, and 2920 A°, were observed in a microwave discharge through each of the chlorine-containing gases examined. Two continua, with intensity maxima at 2500 and 3050 A°, also appeared. These features are illustrated in Fig. 3. The bands at 2714 and 2920 A° are much weakerthan the other two, and do not appear strongly in the figure. The four clusters of bands have been attributed to the CCl radical,[24, 27-31] and the continua to a transition in the Cl_2 molecule.[32,33] Asundi, Singh, and Mishra[33] observed two additional emission continua, with intensity maxima at 4000 and 3340 A°, in a low frequency discharge through CCl_4, but these continua were not found with a microwave discharge, as used in the work described in this thesis. The above three authors assigned the latter two continua to a transition occuring in the decomposition of CCl_4 into CCl and other products.

(b) An extensive system, consisting of forty-five violet-degraded bands between 2370 and 3231 A°, was observed when any fluorine-containing gas was excited. These bands have many close heads, and are superimposed on a continuous background which extends from the short wavelength limit of observation (about 2400 A°) to 3500 A°. The intensity maximum appears to be at 2650 A°, but actually may be at a lower wavelength, as the light emitted near 2400 A° was diminished in intensity because of absorption by the optical filter.

The discrete bands comprise all but the weakest features of the CF_2 emission spectrum reported by Venkateswarlu[2] and by Johannin-Gilles.[3] This spectrum is described in Table 1, and many of the observed bands are shown in Fig. 4. Because of the poor contrast with which these bands appear against the continuous background, it was not possible to record all of them in a single exposure. Different conditions of excitation and different exposure times were necessary to photograph the stronger and weaker features respectively.

The continuum described above possibly may be identified with the continuous emission observed by Gale and Monk[34] in a discharge through F_2. These authors reported intensity maxima at 2600 and 2800 A°. When $CBrF_3$ was excited in the microwave discharge, the continuous background extended to longer wavelengths, ending at about 4400 A°. An identical continuum was found when pure bromine was excited under the same conditions. This feature has been assigned by Venkateswarlu[35] to transitions between stable upper and repulsive lower states of Br_2, and is analagous to the transition giving rise to the Cl_2 continua described in (a).

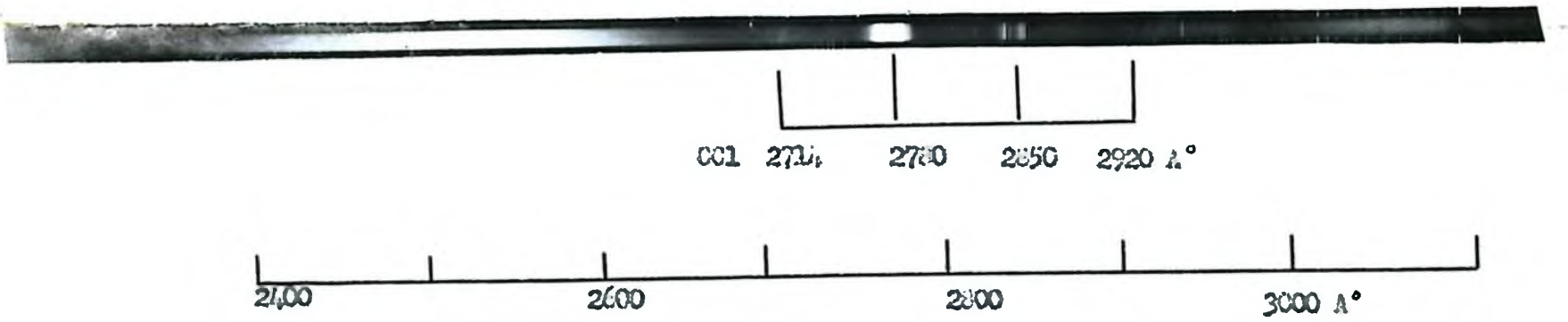

Fig. 3. CCl Emission Bands and Associated Continua. The weak bands at 2714 and 2920 A° can barely be seen. They appear only with very long exposures.

TABLE 1.

WAVELENGTHS AND INTENSITIES OF THE CF_2 BAND HEADS

The heads from 2399.2 to 3249.5 A° were observed by Venkateswarlu,[2] and the numbers in brackets are his visual intensity estimates. The first five heads were observed by Johannin-Gilles.[3] Those marked # were also obtained in absorption by Barrow.[4] The heads marked * were observed in the work described in this thesis.

2328 A°

2345 A° #

2355 A°

2371 A° * #

2381 A° *

2399.2 A° (0) * #

2409.4 A° (0)

2428.3 A° (3) * #

2438.5 A° (2)

2457.6 A° (7) * #

2467.8 A° (2)

2472.3 A° (2) *

2487.8 A° (9) * #

2502.6 A° (2) *

2518.7 A° (9) * #

2530.0 A° (2)

2541.3 A° (3)

2550.6 A° (8) * #

2561.8 A° (4) *

2573.2 A° (4) *

2583.6 A° (3) * #

2594.6 A° (9) *

2594.96 A° (?)

2606.7 A° (2)

2617.9 A° (3) #

2628.5 A° (9) *

2652.4 A° (6) * #

2663.4 A° (4)

2675.5 A° (6) *

2688.1 A° (5) *

2699.1 A° (3)

2711.3 A° (9) *

2736.4 A° (8) *

2749.1 A° (4) *

2761.2 A° (5) *

2774.2 A° (5) *

2787.1 A°(3) *
2799.8 A°(8) *
2812.9 A°(2)
2839.4 A°(2) *
2852.5 A°(6) *
2866.1 A°(6) *
2879.7 A°(4) *
2893.5 A°(7) *
2907.5 A°(3)
2921.3 A°(6) *
2935.2 A°(3) *
2949.8 A°(2)
2978.9 A°(2) *
2993.7 A°(2) *
3007.5 A°(3) *
3022.8 A°(5) *
3038.1 A°(5) *
3053.7 A°(5) *
3069.6 A°(3) *
3084.6 A°(2) *
3164.6 A°(1) *
3181.0 A°(2) *
3197.5 A°(4) *
3214.1 A°(6) *
3231.1 A°(2) *
3249.5 A°(1)

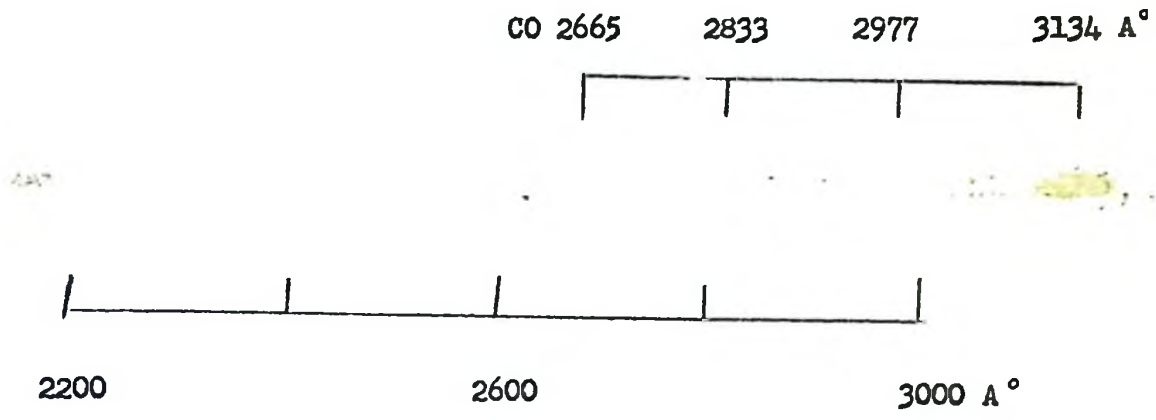

Fig. 4. CF_2 Emission Bands and Impurity Spectra, 2400 - 3200 A°. A contact print, rather than an enlargement is shown in order to produce the best contrast.

(c) The (0-0) band of a $^2\Delta - ^2\pi$ transition of CH was observed at 4315 A° when hydrogen-containing Freons were excited.[36] As this spectrum has been thoroughly investigated by other workers, it was of no further interest.

(d) The spectra of several impurities, CO, C_2, and CN, were excited by discharges through the Freons. These spectra are described in Table 2, and illustrated in Figs. 4 and 5a.* They were identified by comparison with the spectra described by Pearse and Gaydon.[36] The intensity of the C_2 bands increased with higher partial pressures of the Freons, and became especially intense when the discharge tube walls became heavily coated with a graphite-like deposit after prolonged use. Undoubtedly the carbon molecules were formed by the decomposition of the Freons. Carbon monoxide is frequently excited as an impurity in the positive column of discharges, being given off by the glass walls of the tube.[36] Its spectrum increased in intensity at lower total pressures. The CN bands appeared only when helium was being used, and were reduced in intensity when the helium was purified by passing it through a charcoal trap at low temperatures to remove nitrogen impurities.

The visible glow given off by the discharge was entirely due to these impurities, as the CF_2 and CCl spectra are found in the ultraviolet. At high partial pressures of the Freons, this glow was bluish-white, becoming whiter as the total pressure was lowered.

*The impurity spectra were not usually as intense as in Figs. 3, 4, 5 and 6. These photographs were overexposed in order to study the impurity emission.

TABLE 2.

IMPURITY SPECTRA OBSERVED IN DISCHARGES THROUGH FREONS

CO Third Positive and 5B Bands: These are violet-degraded bands, each with five close sub-heads. Heads were found at the following wavelengths:

2665.3 A°	3134.4 A°
2833.1	3242.1
2977.4	3305.7

CO Angstrom Bands: The heads of these violet-degraded bands were found at the following wavelengths:

4510.9 A°	5610.2 A°
4835.3	6079.9
5198.2	

C_2 Swan Bands: These violet-degraded bands had heads at 5635.5 and 5165.2 A°.

CN Violet-Bands: The heads of these violet-degraded bands were found at the following wavelengths:

3861.9 A°	4181.0 A°
3871.4	4197.2
3883.4	4216.0

TABLE 3.

OBSERVED ATOMIC LINES OF HELIUM

2723.3 A°	3867.5 A°	4437.5 A°
2763.8	3888.7	4471.5
2829.1	3964.7	4713.1
2945.1	4009.3	4921.9
3187.7	4026.2	5015.7
3705.0	4120.8	5047.7
3732.9	4143.8	5875.7
3819.6	4387.9	

TABLE 4.

IMPURITY SPECTRA OBSERVED AT HIGH PARTIAL PRESSURES OF HELIUM

CO^+ First Negative Bands: These are red-degraded bands with heads at the following wavelengths:

2419.4 A°	2557.7 A°	2722.4 A°
2445.8	2607.2	2752.9
2474.2	2638.8	2785.8
2504.6	2672.4	2820.8
2550.3		

CO_2^+ Bands: Two very sharp band heads are found at 2883 and 2896 A°.

N_2^+ Bands: In addition to violet-degraded bands with heads as listed below, a number of close lines were observed between 3050 and 3300 A°. Pearse and Gaydon[36] show these same lines in their reproduction of the N_2^+ spectrum.

3914.4 A°	4236.5 A°	4554.1 A°
4166.8	4278.1	4599.7
4199.1	4515.9	4651.8

Sodium Atomic Lines: These lines appeared as close doublets.

6160.8 A°	5153.6 A°	4668.6 A°
6154.2	5149.1	4664.9
5895.9	4982.8	
5889.9	4978.6	

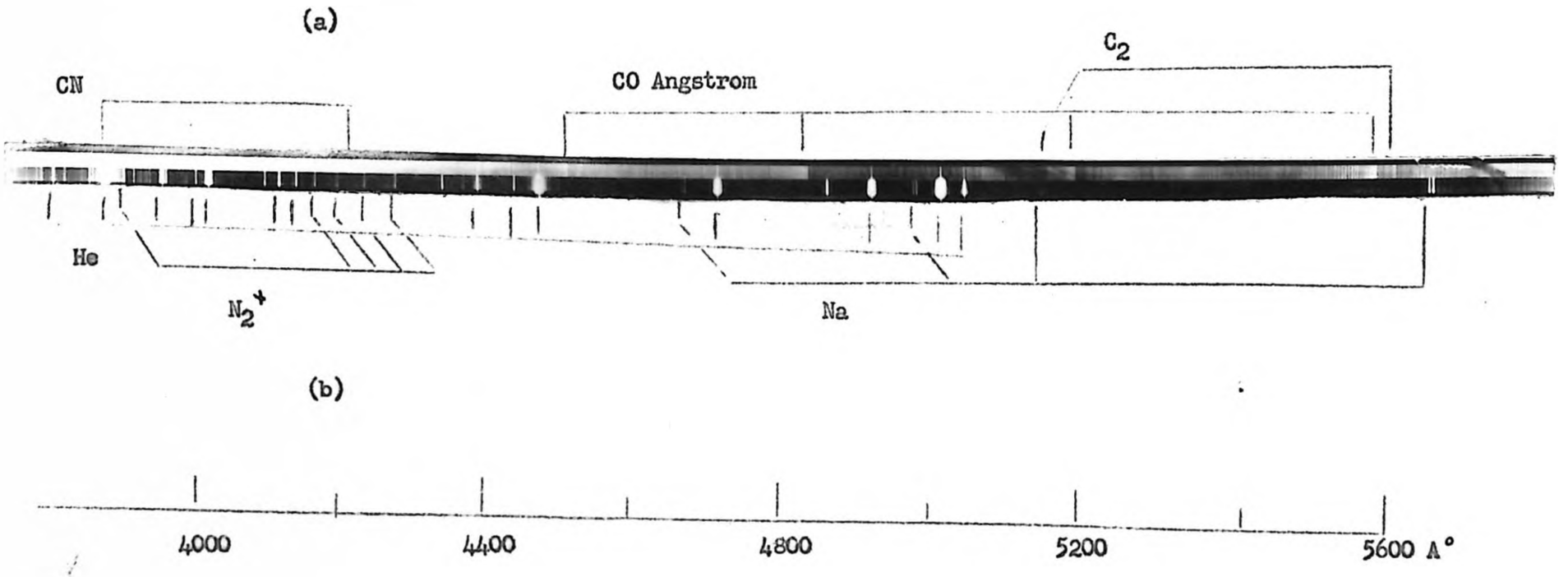

Fig. 5. Impurity Spectra, 3700 - 5700 A°. (a) CF_4 in helium. (b) Pure helium.

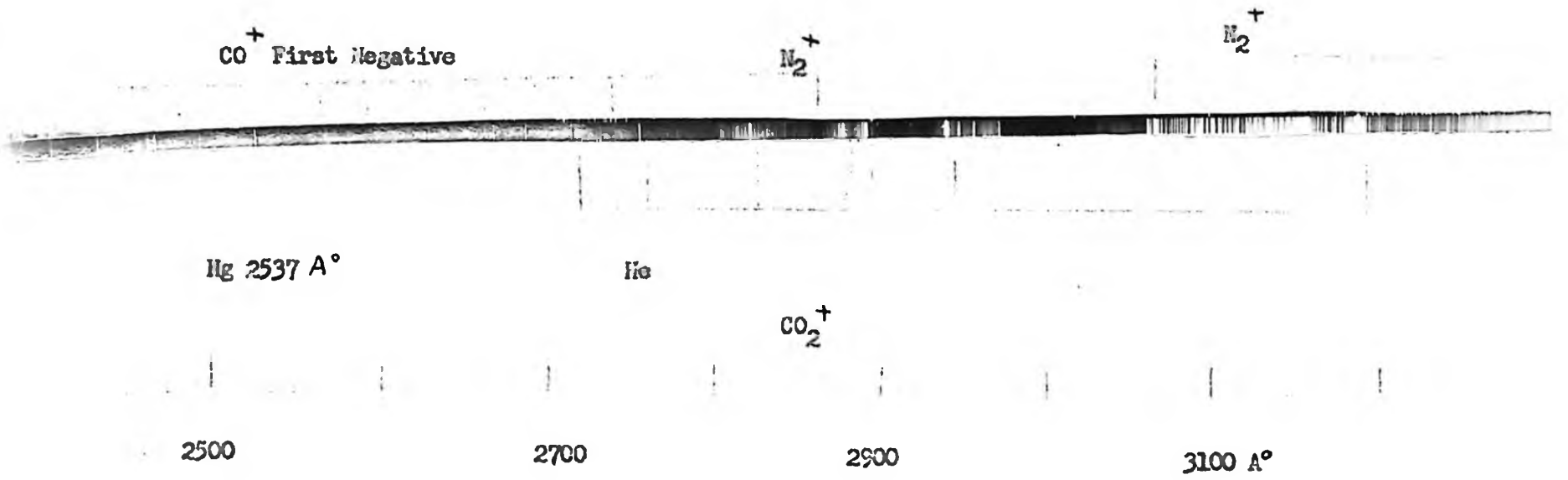

Fig. 6. Impurity Spectra in Pure Helium, 2400 - 3300 A°.

(e) When the ratio of helium to Freon in the gas mixture being excited was very high, or when pure helium was excited, the visible glow took on a rose colour. This was due to several very intense emission lines of helium.[37] The observed line spectrum of helium is listed in Table 3, and shown in Figs. 5b and 6. No lines of the ionized helium atom were observed.

At high partial pressures of helium, different impurity spectra were found.[36] The spectra of C_2 and CN disappeared, as they depend on the formation of carbon in the decomposition of the Freons. The new impurity spectra were due to the ionized species CO^+, CO_2^+, and N_2^+. Atomic lines of sodium were also observed, the sodium having come from the glass walls. These spectra are described in Table 4 and illustrated in Figs. 5b and 6.

The excitation of ionic impurities at high partial pressures of the carrier gas is due to the fact that the lowest excited states of helium are metastable and lie at unusually high energies. The lowest is 19.72 eV above the ground state.[38] Under these conditions almost all the collisions of the electrons are with helium atoms, and few electrons are able to lose energy until they can excite helium. The excited helium atoms cannot return to the ground state by emitting light. In their metastable states, they can lose energy only by collision. As the ionization potentials of CO, CO_2, and N_2 are of the order of 15 eV,[37] collision with these impurity molecules lead to ionization. On the other hand, at higher partial pressures of the Freons, most of the electrons collide inelastically with Freon molecules, and never gain sufficient energy to excite helium atoms. This effect is demonstrated by a sharp decrease in the intensity of the helium line spectrum when Freon is added to the discharge. (Compare Figs. 5a and 5b.)

(f) The spectrum observed in the microwave excitation of $CBrF_3$ differed from that obtained with other fluorine-containing gases only in that a continuum due to Br_2 appeared, as described in section (a). Quite different results, however, were obtained with the low frequency excitation of this Freon.* The visible glow was a butter yellow. Continuous emission, with intensity maxima at 2650 and 5700 A°, was found throughout the entire observed spectral region, (2400-6500 A°). The short-wavelength portion of this continuum is identical to that observed in the microwave discharge through this gas. [see section (a)]. The higher wavelength portion, with its very intense maximum at 5700 A°, could not be explained. It was thought that it might have been emitted by the bromine which was formed in the discharge; however, when pure bromine was excited under the same conditions, only the lower wavelength continuum due to Br_2^{35}, and a system of red-degraded bands between 5100 and 6400 A° due to Br_2^{+} [39] were observed. Continuous emission due to the recombination of bromine atoms is known,[40] but not at wavelengths greater than 5100 A°. It may be that 5700 A° continuum is due to the dissociation of the $CBrF_3$. In any case, the results obtained in the low frequency excitation of $CBrF_3$ show that different conditions of excitation can lead to different spectra.

The result of this preliminary work is that the emission spectra of the CCl, CH, and CF_2 radicals were observed under low resolution. No

*The low frequency excitation was studied in the same tube used for microwave work, with external electrodes connected to a high-voltage transformer. The same yellow glow appeared under these conditions, with the Schuler tube, and with Tesla coil excitation. With the Schuler tube, however, there were very intense impurity spectra. The intensity of emission with Tesla coil excitation was too low to photograph.

discrete spectra arising from other free radicals were observed. A number of other spectral features were found and were of some interest in considering the nature of the excitation processes. These processes, however, are very complex, and are not well understood at the present time.

CHAPTER 5.

ANALYSIS OF THE CCl EMISSION SPECTRUM: INTRODUCTION AND HISTORICAL REVIEW

The remainder of this thesis is devoted to the detailed study made of the emission spectrum of the CCl radical. It has already been described how this spectrum was photographed under low resolution. Succeeding chapters describe how the two more intense groups of bands, at 2780 and 2850 A°, were photographed under high resolution, and how rotational and vibrational analyses were performed. The present chapter describes previous investigations of this spectrum by other workers.

Jevons[27] in 1924 studied the emission spectrum of flowing CCl_4 vapour in an uncondensed electric discharge, and observed violet-degraded bands at 2788 and 2777 A°, as well as other bands due to CO and C_2.

Repeating the experiment in 1937, Asundi and Karim found the prominent features reported by Jevons, and in addition weaker clusters of bands at 2714 and 2850 A°. They also reported a number of continua, most of which were due to Cl_2, but two of which they thought might be due to the decomposition of the CCl_4 molecule.[33] These continua were discussed in Chapter 3. On the basis of the doublet structure of the three clusters of bands, and by analogy to the spectrum of SiF,[41] these workers identified the bands obtained in CCl_4 with a $^2\Sigma - {}^2\Pi$ transition of the diatomic CCl molecule. They arranged the observed band heads in a vibrational scheme.

Two years later Horie,[29] using a condensed discharge in CCl_4, observed two additional band heads at 2920.7 and 2927.5 A°. He agreed that the spectrum resulted from a $^2\Sigma - {}^2\Pi$ transition of CCl, but proposed a somewhat different vibrational analysis.

The CCl spectrum was further investigated by Venkateswarlu,[30] using a 21 ft. grating spectrograph for the more intense bands, and a smaller instrument for the weaker features. He reported seeing rotational structure, but with insufficient resolution to perform a rotational analysis. Like Horie, he considered that the four clusters of double-headed bands at roughly 2714, 2780, 2850, and 2929 A° were the $(v' - v'') = 1, 0, -1$, and -2 sequences* respectively of a $^2\Sigma - {}^2\Pi$ transition of CCl. Within these clusters, however, he found several new band heads which did not fit into previous vibrational analyses, and he proposed a new interpretation.

Finally, in 1959, Kuzyakov and Tatevskyi[24,31] examined this spectrum with higher resolution and performed a partial rotational analysis of the most intense bands at 2780 and 2850 A°. They pointed out several inconsistencies in Venkateswarlu's vibrational analysis, and proposed still another. They, too, attributed the system to a $^2\Sigma - {}^2\Pi$ transition.

It should also be noted that the more intense CCl bands have been observed in the internal cone of the flame of some halogenated organic compounds burning in air or oxygen,[42] and in an electrical discharge through $CHCl_3$, CCl_3CHO, and $C_6H_5CCl_3$.[26]

*A sequence is a series of bands for each of which the difference $(v' - v'')$ of initial and final state vibrational quantum numbers is constant.

Barrow[26] and Kuzyakov and Tatevskyi[25] observed another band system in an uncondensed discharge through CCl_4. It consists of red-degraded bands in the region 2338-2446 A°, with an intensity of about one tenth that of the system described above. Unlike the previous system, it does not have a double-headed structure. It is thought to be due to a $^2\Sigma - ^2\Sigma$ transition in CCl, or a singlet-singlet transition in CCl^+. The latter workers favoured the ion as the emitter, on the grounds that the occurrence of the spectrum is favoured by relatively severe conditions of excitation. They arranged the band heads in a Deslandre's table, but no rotational analysis was performed. This system was not found in the work described in this thesis, as all the more intense bands lie outside the spectral region which could be investigated.

CHAPTER 6.

PRODUCTION AND MEASUREMENT OF THE EMISSION SPECTRUM OF CCl UNDER HIGH RESOLUTION

It was seen in Chapter 3 that the emission spectrum of CCl, consisting of four clusters of bands at 2714, 2780, 2850, and 2920 A^{o}, could be observed when any chlorine-containing Freon was excited in a microwave discharge. This chapter describes how the two most intense bands, at 2780 and 2850 A^{o}, were photographed under high resolution.

A rose-coloured glow was excited in helium flowing at 0.1 mm. pressure through the microwave discharge tube described earlier, and just enough CCl_4 vapour was added to the streaming gas to change the colour of the discharge glow to a bluish-white. Under these conditions, an average exposure time of four hours was required to photograph the bands on Kodak 103a0 glass plates, although this period lengthened with the age of the discharge tube. An iron arc was used to provide a comparison spectrum.

The high resolution studies were performed in the second order of a 20 ft. Ebert grating spectrograph.[43] Attempts to obtain better resolution by working in the third order failed because of the very high grating angle required. A rectangular stop, with razor blade edges, was placed between the spectrograph and the discharge tube to match their respective optical apertures, and thus eliminate unwanted stray light. Since resolving power depends on the area of the grating, it was desirable to illuminate evenly the entire ruled surface. The stop was just large enough to do this.

The theoretical second-order resolving power of the spectrograph was 300,000, which means that in the 35,500 $cm.^{-1}$ region which was being examined, it should be possible to resolve lines with a separation of 35,500/300,000 = 0.12 $cm.^{-1}$ In practice, lines separated by 0.15 $cm.^{-1}$ were resolved, indicating an actual resolving power of 240,000. The frequency of each line was calculated to $\pm$ 0.001 $cm.^{-1}$, a precision not warranted by the resolution obtained, but in the final results proper allowances were made for errors and uncertainties.

The plates used in the analysis were measured on a travelling microscope. Each plate was measured once in each direction, and in each run three independent measurements of the position of each line were made. The resulting six values were averaged. Wavelengths of the iron arc calibration lines were taken from the MIT Tables,[44] using wherever possible lines whose wavelengths had been determined interferometrically.

The wavelength dispersion of the spectrograph, that is the relation between wavelength in air and position on the plate of a given spectral line, was not quite linear. A correction formula, discussed by Callomon,[46] and based on the geometry of the spectrograph, was used to allow for this nonlinearity. The wavelengths in air thus obtained were converted to wavelengths in vacuum using Edlen's tables.[45] Finally, the vacuum wavelengths were converted to vacuum wavenumbers. These three operations were combined to give a direct conversion from position on the plate to vacuum wavenumber. A small correction, which did not exceed 0.7 $cm.^{-1}$, was added to a linear equation connecting the two variables. The linear equation was based on the positions of

only two iron arc lines, but the correction was so designed as to account for the deviations of the other iron arc lines from the linear equation.

The high resolution spectrograms are shown in Fig. 7. Microdensitometer profiles of these spectrograms are reproduced later in this thesis.

Very small differences in temperature warp the steel casing of the spectrograph, shifting the position of the plate during an exposure and broadening the lines. For this reason, the spectrograph was heavily insulated with fibreglass, and the laboratory was thermostatted to $\pm$ 0.1 C. Fluctuations in atmospheric pressure can also destroy the resolution by changing the refractive index of air. To check for possible effects of this sort, adjacent iron arc spectra were photographed on the same plate at intervals of four to twelve hours.

Since no shift of the lines was observed, it may be assumed that such temperature and pressure effects were negligible.

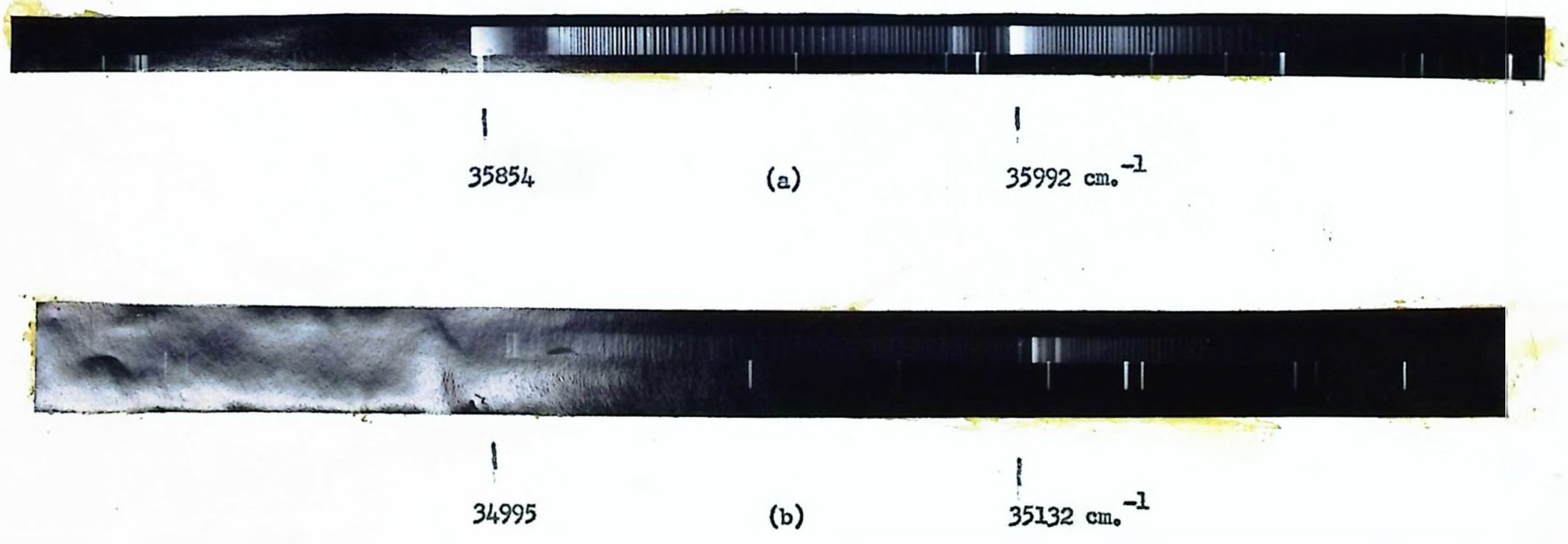

Fig. 7. High-Resolution Spectrograms of the CCl Spectrum at (a) 2780 and (b) 2850 A°.

CHAPTER 7.

ROTATIONAL ENERGY LEVELS AND SPECTRA OF DIATOMIC MOLECULES IN DOUBLET STATES

This chapter gives an account of the rotational energy levels of a diatomic molecule, and a description of the transitions between these levels, with special reference to the CCl spectrum. The material discussed has been drawn chiefly from the work of Herzberg,[47] Johnson,[48] Mulliken,[49,50] Van Vleck,[51,52] and their co-workers.

I. ROTATIONAL ENERGY LEVELS IN HUND'S CASES (a) AND (b);- The energy of a molecule is the sum of electronic, vibrational, rotational, and translational contributions. The latter need not be considered if internal coordinates attached to the molecule are used. The vibrational energy can be treated separately. Here the electronic and rotational energies are first discussed, and the effect on these energies of interactions between rotational and electronic motions is then introduced.

Classically, a rigid body has rotational energy

$$E = \underline{P}_x^2 /2I_x + \underline{P}_y^2 /2I_y + \underline{P}_z^2 /2I_z \qquad (1)$$

where $\underline{P}_i$ and I_i are the components of angular momentum and moments of inertia respectively about the three Cartesian axes x, y, and z, with the origin at the centre of mass. In a diatomic molecule, with z along the internuclear axis, $I_x = I_y \gg I_z$, since I_z is due entirely to electrons. The molecule is thus a prolate symmetric top and is shown in Fig. 8. $\underline{J}$ is a vector representing the total angular momentum of the molecule. Its component $\underline{R}$, perpendicular to the molecular axis,

represents the angular momentum due to rotation of the nuclei about their centre of mass. Hence, $\underline{N}^2 = \underline{P}_x^2 + \underline{P}_y^2 = \underline{J}^2 - \underline{P}_z^2$, and the energy is

$$E = (\underline{J}^2 - \underline{P}_z^2)/2I_x + \underline{P}_z^2/2I_z. \qquad (2)$$

According to quantum theory, the angular momenta $\underline{J}$ and $\underline{P}_z$ are quantized. The magnitude of $\underline{J}$ is $(h/2\pi)\sqrt{J(J+1)}$, and the magnitude of $\underline{P}_z$, the component of $\underline{J}$ along the molecular axis, is $(h/2\pi)P_z$, where J and P_z are quantum numbers.* Thus, if $B = h/8\pi^2 cI_x$, and $C = h/8\pi^2 cI_z$, the energy in $cm.^{-1}$ is

$$F = E/hc = B\left[J(J+1) - P_z^2\right] + CP_z^2. \qquad (3)$$

This semi-classical treatment yields the same energy expression as a solution of the wave equation for the symmetric top.[47]

The vector $\underline{P}_z$ represents electronic angular momentum; hence, the final term in equation (3) may be included with the electronic energy. For a non-rigid rotator, the energy becomes

$$F(J) = B_v\left[J(J+1) - P_z^2\right] - D_v J^2 (J+1)^2. \qquad (4)$$

As rotational energy increases, the internuclear distance is lengthened by centrifugal forces, and the term in D_v accounts for the corresponding change in moment of inertia. The subscript v indicates the vibrational level for which the rotational constants B and D apply. The mean square of the internuclear distance, from which the moment of inertia is calculated, increases with increasing vibrational energy, and hence B and D differ between vibrational states.

The origin of the electronic angular momentum $\underline{P}_z$ about the internuclear axis must now be considered. In an atom, the total angular momentum due to orbital motion of the electrons may be represented by

*Underlined symbols are used to denote vectors. The same symbols, not underlined, denote their associated quantum numbers.

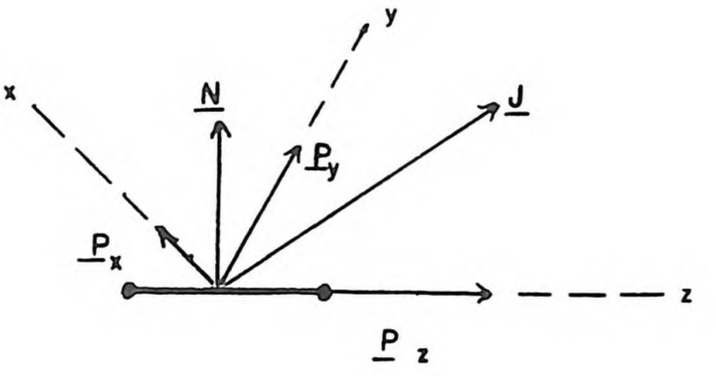

Fig. 8. The Diatomic Molecule as a Symmetric Top.

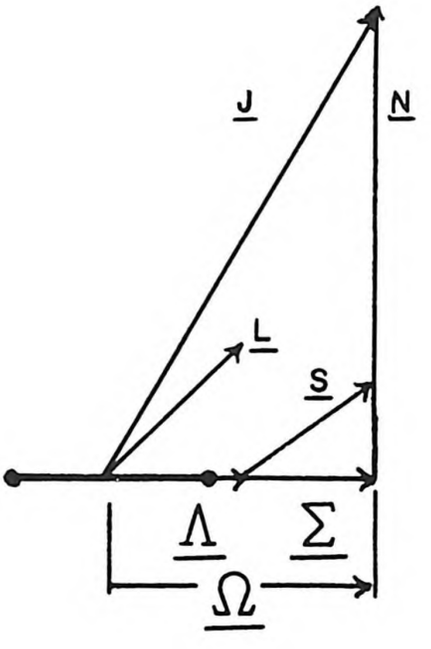

Fig. 9. Coupling in Hund's Case (a).

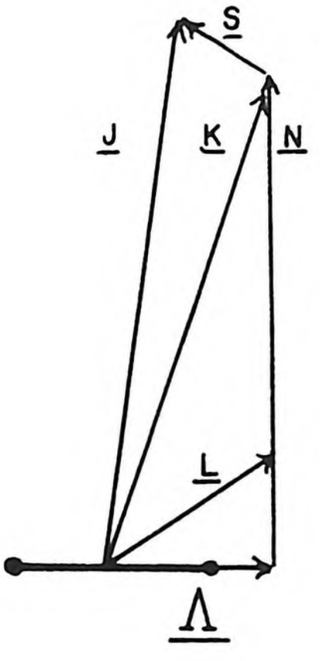

Fig. 10. Coupling in Hund's Case (b).

a vector $\underline{L}$ which, neglecting the effects of electron spin, is a well-defined constant of the motion. In a diatomic molecule, the electric field in which the electrons move loses the spherical symmetry of the atom and becomes axially symmetric about the internuclear axis. In such a field $\underline{L}$ processes about the internuclear axis. The velocity of precession is so great that $\underline{L}$ is no longer a constant of the motion, and only its component M_L along the internuclear axis remains well defined.* As this results from electrostatic interactions, there is no energy difference associated with opposite directions of precession, that is with opposite signs of M_L. Thus $\Lambda = |M_L|$ replaces L as a valid quantum number, and states with $\Lambda \neq o$ are doubly degenerate.** Electronic states are designated Σ, Π, Δ, etc. when $\Lambda = 0, 1, 2,$ etc. respectively.

A vector $\underline{S}$ describes the total angular momentum arising from the spins of unpaired electrons in the molecule. In CCl, which has twenty-three electrons, one, or possibly three, of them are expected to be unpaired, giving rise to a doublet, or possibly a quartet, electronic state. That the observed CCl spectrum involves doublet states is apparent from the double-headed structure of the bands shown in Fig. 7. This discussion is therefore limited to doublet electronic states, and the quantum number $S = \frac{1}{2}$.

---

*The time-averaged magnitude of the component of $\underline{L}$ perpendicular to the internuclear axis is zero.

**It must be noted that two such degenerate states do not in fact correspond to opposite directions of precession of $\underline{L}$. A solution of the wave equation for the system yields two eigenfunctions, $\Psi(+)$ and $\Psi(-)$, belonging to the same eigenvalue and corresponding to opposite directions of precession of $\underline{L}$. Any linear combination of these two functions, however, is also a valid wave function. Thus the two degenerate states must be considered as having eigenfunctions $\Xi_1 = \Psi(+) + \Psi(-)$ and $\Xi_2 = \Psi(+) - \Psi(-)$, and neither state may be associated exclusively with a given direction of precession of $\underline{L}$.[47]

An interaction between the magnetic moments due to $\underline{S}$ and to $\underline{\Lambda}$ causes $\underline{S}$ to precess about the internuclear axis with a component $\Sigma = \pm \frac{1}{2}(h/2\pi)$ along that axis. Since the interaction is magnetic, there is an energy difference between states in which $\underline{\Lambda}$ and $\underline{\Sigma}$ are parallel or antiparallel. As shown in Fig. 9, $\underline{\Lambda}$ and $\underline{\Sigma}$ add to form $\underline{\Omega}$, and the latter vector is identical to $\underline{P}_z$ of Fig. 8. The rotational energy of the molecule is thus given by

$$F(J) = B_v \left[J(J+1) - \Lambda^2\right] - D_v J^2 (J+1)^2 \pm \tfrac{1}{2} A \Lambda \qquad (5)$$

where $J = \Omega, \Omega+1$, etc. The final term is the energy of interaction of $\underline{\Sigma}$ and $\underline{\Lambda}$. A is called the spin-orbit coupling constant, and the factor $\frac{1}{2}$ is the quantum number Σ. According to this model, a doublet electronic state with $\Lambda \neq 0$ has two sets of rotational levels. Levels with the same J have a separation of $A\Lambda$. The two sub-states are designated by a subscript showing the value of $|\Lambda + \Sigma|$, for example $^2\Pi_{\frac{1}{2}}$ and $^2\Pi_{3/2}$. In regular states where A is positive, the sub-state with the lower value of $|\Lambda + \Sigma|$ is lower in energy. In inverted states A is negative, and the order of the levels is reversed.

In a Σ state, where $\underline{\Lambda} = 0$, $\underline{S}$ cannot be coupled to the molecular axis, and the quantum number Σ is not defined. Here, levels of the same J are degenerate.

The model just presented is valid only if there is no appreciable interaction between nuclear rotation and electronic motion. Such an interaction modifies the way in which the vectors are coupled. It is convenient to discuss these modifications in terms of idealized limiting cases called Hund's coupling cases.

In Hund's case (a) it is assumed that the interaction between nuclear rotation and electronic motion is negligible, while $\underline{L}$ and $\underline{S}$

are each strongly coupled to the internuclear axis. In other words, the above model is a valid description, and equation (5) gives the correct energy. As noted above, a Σ state cannot belong to case (a).

The opposite assumptions are made in case (b). Here the rotation of the nuclei is considered to be more rapid than the precession of S about the internuclear axis. S is uncoupled from the internuclear axis and Σ is no longer defined. Fig. 10 shows how Λ and R form a resultant K which is loosely coupled with S to give the total angular momentum J. The quantum number K takes on the values Λ, $\Lambda+1$, etc. In this approximation there is no magnetic moment in the direction of K with which S may interact, and therefore levels of equal K are degenerate. The energy may be derived by the same argument that led to equation (4), and is given by

$$F(K) = B_v \left[K(K+1) - \Lambda^2\right] - D_v K^2(K+1)^2. \qquad (6)$$

Case (b) is the appropriate model for a Σ state. For states in which $\Lambda \neq 0$, case (a) provides a valid description at low J values, but as the rotaional energy increases, and S is uncoupled from the internuclear axis, case (b) assumptions become more appropriate.

Hill and Van Vleck[51] have derived an expression for the rotational energy of a diatomic molecule with any form of coupling intermediate to cases (a) and (b). Starting with case (b) assumptions, they introduced the coupling between S and Λ as a perturbation. Their expression for a doublet state is

$$\left\{\begin{matrix} F_1(J) \\ F_2(J) \end{matrix}\right\} = B_v \left[(J+\tfrac{1}{2})^2 - \Lambda^2 \mp \sqrt{(J+\tfrac{1}{2})^2 + Y(Y-4)\Lambda^2/4}\right] - D_v \left\{\begin{matrix} J^4 \\ (J+1)^4 \end{matrix}\right\} \qquad (7)$$

where $Y = A/B_v$. The two expressions, $F_1(J)$ and $F_2(J)$, are obtained

by using the upper and lower signs respectively. The first gives the energy of rotational levels in which $J = K + \frac{1}{2}$, and the second is used for the levels in which $J = K - \frac{1}{2}$.* For the lowest value of J (i.e. $J = \Lambda - \frac{1}{2}$), there is just one state, since, in case (a), the lowest value which J may take is Λ. For this one level, the expression F_1 is used for $2 < Y < +\infty$, and the expression F_2 for $-\infty < Y < 2$.

In Fig. 11, a correlation is made between the rotational energy levels of a $^2\Delta$ state as Y is varied from large positive to large negative values.[53] This change in Y corresponds to the transition $^2\Delta\,(a)_{reg} - {}^2\Delta\,(b) - {}^2\Delta\,(a)_{inv}$. The correlation diagram shows how case (b) levels of equal K are approximately degenerate, while case (a) levels of equal J have a constant separation. The order in which the various levels lie for any degree of coupling, that is for any value of Y, is also shown.

In Appendix I it is shown how the Hill and Van Vleck expression (equation 7) reduces to the case (a) and case (b) expressions, given by equations (5) and (6) respectively, if appropriate assumptions are made as to the relative values of Y and J. Equation (7) is also reduced to forms suitable for a description of the energy levels observed in CCl.

Other coupling cases have been described[47,49] in which $\underline{S}$ and $\underline{L}$ are more strongly coupled to each other than to the internuclear axis, or in which $\underline{\Lambda}$ is not defined. The latter situation arises chiefly in hydrides where the deviation of the electric field from the spherical

*In case (a), K is not defined. Which of the two energy expressions is to be used for a given rotational level must then be determined by making a correlation between that level and the corresponding case (b) level, with the aid of Fig. 11.

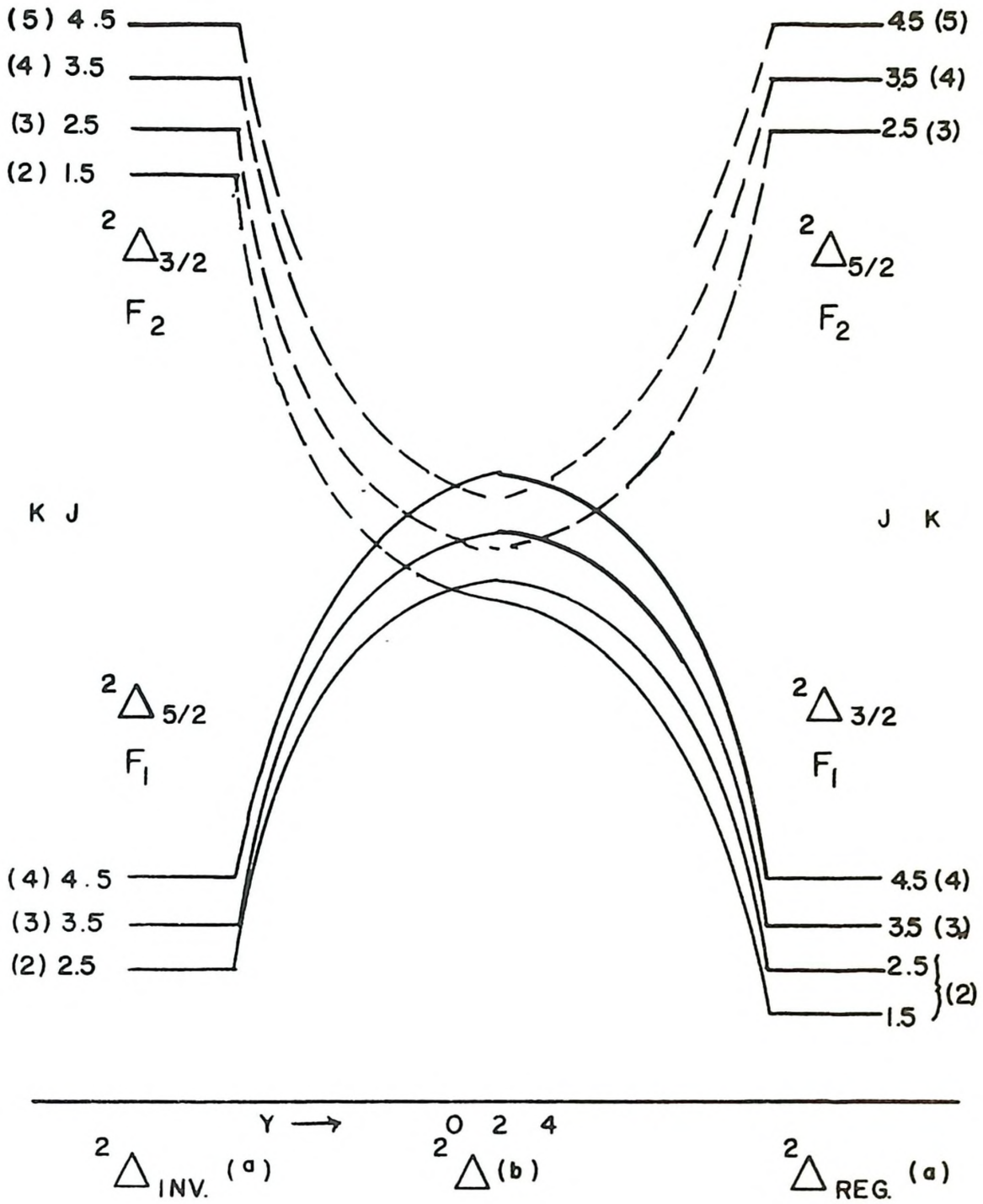

Fig. 11. Correlation Between Cases (a) and (b). F_1 levels are shown by solid lines, and F_2 levels by broken lines.

symmetry of the united atom is not pronounced. Cases (a) and (b), however, are adequate for a description of the CCl spectrum. Case (d) is mentioned below in connection with Λ-type doubling.

II. SPIN DOUBLING IN CASE (b) STATES:- It has been assumed thus far that in a Σ state, case (b) conditions apply exactly, and that levels with the same K are degenerate for all values of K. Actually, there are small interactions which remove this degeneracy.[47,52] The rotation of the nuclei about their centre of mass causes a distortion of the precession of $\underline{L}$, such that the velocity of precession is not uniform. The time-averaged magnitude of the component of $\underline{L}$ perpendicular to the internuclear axis therefore does not vanish, and a small magnetic moment is set up in the direction of $\underline{K}$. To this is added a small magnetic moment in the same direction due to the rotation of the charged nuclei. The latter is only a small fraction, (mass, electron)/(mass, nuclei), of the magnetic moments which arise from electronic motion. These two moments interact with $\underline{S}$ to produce a splitting of levels of equal K as follows:

$$\begin{aligned} F_1(K) &= F(K) + \tfrac{1}{2}\gamma K \\ F_2(K) &= F(K) - \tfrac{1}{2}\gamma (K+1) \end{aligned} \qquad (8)$$

where F(K) is the energy given by equation 6, and γ is a very small constant.

This spin splitting can also occur in case (b) states with $\Lambda \neq 0$, but it is a much smaller effect than the splitting of levels having case (a) tendencies.

III Λ-TYPE DOUBLING:- Λ-type doubling is the removal of the two-fold degeneracy of all states in which $\Lambda \neq 0$. The Λ-type doubling of

a case (a) or (b) state may be thought of as a slight tendency towards case (d) coupling.[47,51]

In case (d) it is assumed that $\underline{L}$ is coupled only weakly to the internuclear axis, but that there is a strong interaction between $\underline{L}$ and $\underline{N}$. These two vectors combine to form $\underline{K}$, which, as in case (b), is the total angular momentum apart from spin. $\underline{K}$ and $\underline{S}$ add to form $\underline{J}$ as shown in Fig. 12. The rotational energy is given to a first approximation by

$$F(N) = B_v N(N+1). \qquad (9)$$

Each level with a given N is split into $2L+1$ components, each of which is further split into two close levels corresponding to the two orientations of $\underline{S}$. Since Λ is not defined, a case (d) state is characterized by a constant value of L, rather than by a constant value of Λ. If an adiabatic correlation is made between a case (d) state with $L=1$, and a case (a) or (b) state, the single case (d) state goes over into a Σ and a Π state, corresponding to the two possible values of $|M_L|$. Such a correlation is illustrated in Fig. 13. It can be seen how a slight tendency towards case (d) removes the two-fold degeneracy of each rotational level of the Π state.

Quantum-mechanically, both Λ-type doubling and the spin splitting described in Section II may be thought of as arising from perturbations by neighbouring electronic states. The magnitude of the splitting produced by either type of doubling increases as the energy separating the perturbing and perturbed states decreases.

Herzberg[47] and Mulliken and Christy[50] have discussed the magnitude of Λ-type doubling in different electronic states. In $^2\Pi$ case (b) states it is small, and increases quadratically with J. In $^2\Pi_{\frac{1}{2}}$ case

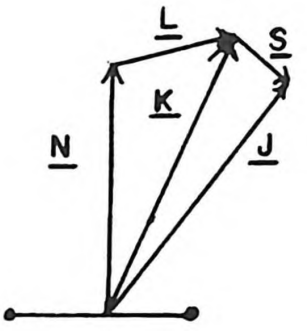

Fig. 12. Coupling in Hund's Case (d).

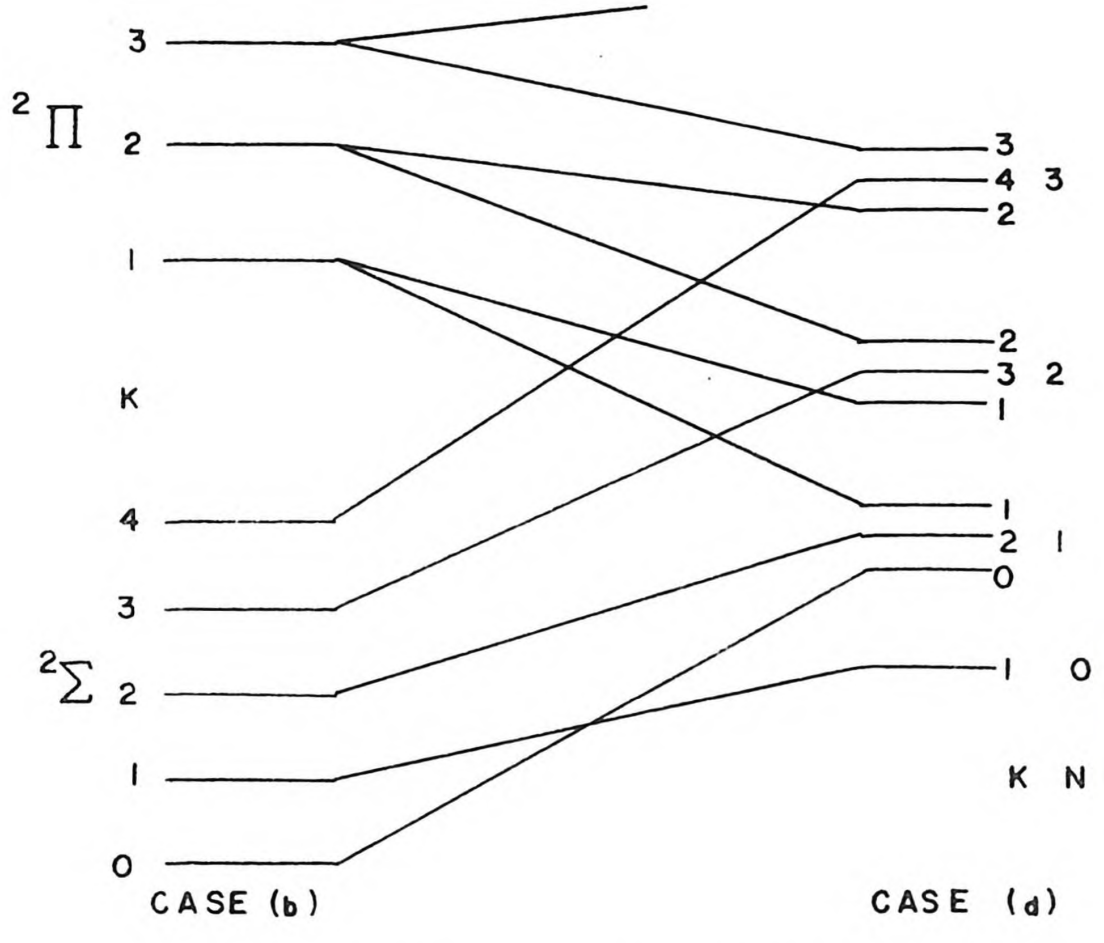

Fig. 13. Correlation Between Cases (b) and (d) for L=1. It is assumed that any spin doubling is negligible.

(a) states it is comparatively large, and increases linearly with J. In $^2\Pi_{3/2}$ case (a) states it increases with the third power of J, but for moderate J it is much smaller than in the corresponding $^2\Pi_{\frac{1}{2}}$ sub-state. Λ-type doubling is negligibly small in Δ states.

IV. SELECTION RULES AND ALLOWED TRANSITIONS:- The allowed transitions* which give rise to the observed spectrum of a molecule are limited by a number of selection rules. The first four rules listed below are perfectly general.

(i) Δ J = -1, 0 or + 1. Spectral lines arising from these three types of transition form respectively the P, Q, and R branches which make up a band.

(ii) $\Delta \Lambda = 0, \pm 1$. This rule forbids transitions of the type $\Sigma - \Delta$. A further provision states that if $\Delta \Lambda = 0$, transitions with Δ J= 0 are weak. Thus, for example, in a $\Pi - \Pi$ transition only the first few lines of a Q branch would appear with appreciable intensity.

(iii) Positive states combine only with negative ones, and vice versa. Each rotational level is classified as positive or negative according to whether its total wave function is unchanged or changes sign by a reflection at the origin. In states with $\Lambda \neq 0$, the two Λ-type components differ in this symmetry classification. It is shown in Fig. 14 how this fact limits the number of spectral lines which arise from the doubling of the levels. If both initial and final states have $\Lambda \neq 0$, each line in the spectrum is doubled. If one

*These rules refer only to electric dipole transitions. Other types of transitions give rise to much weaker spectra.

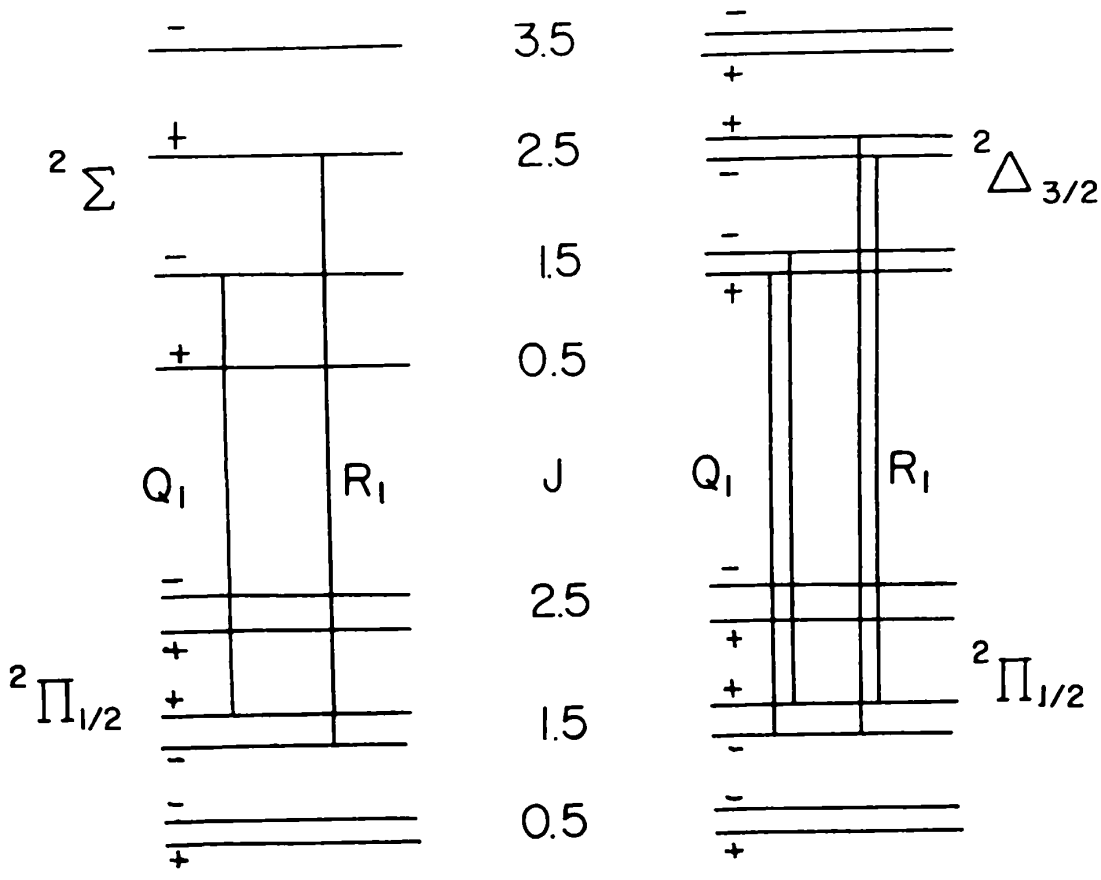

Fig. 14. Λ-type Doubling in Q_1 and R_1 lines.

state is a Σ state, there is no doubling of the lines, but transitions giving rise to certain branches terminate on one set of Λ-components, and transitions giving rise to other branches terminate on the other set.

(iv) $\Delta S = 0$. Transitions between states of different multiplicities are therefore forbidden.

(v) In case (a)-case (a) transitions, where the quantum number Σ is defined in both initial and final states, the rule $\Delta \Sigma = 0$ applies. As a result transitions such as $^2\Pi_{\frac{1}{2}} - {}^2\Delta_{5/2}$ are forbidden, and, neglecting Λ-type doubling, only six branches (two P, two Q, and two R) are allowed in transitions between doublet states.

(vi) In case (b)-case (b) transitions, where K is defined in both initial and final states, only transitions for which $\Delta K = 0 \pm 1$ are allowed, and transitions for which $\Delta K \neq \Delta J$ are of low intensity. Again neglecting the effects of Λ-type doubling, only six branches appear with appreciable intensity. Four additional satellite branches, for which $\Delta K \neq \Delta J$ can appear, but their intensity decreases rapidly with increasing K.

In a case (b)-case (a) transition, neither rules (v) nor (vi) apply. Neglecting Λ-type doubling, twelve branches are now possible, as shown for a typical transition in Fig. 15. The six branches P_1, Q_1, R_1, P_2, Q_2, and R_2 are the main branches which are allowed in (a) - (a) transitions. The four satellite branches Q_{12}, R_{12}, P_{21} and Q_{21} have $\Delta K \neq \Delta J$, and are of low intensity in (b) - (b) transitions. These branches closely parallel four of the main branches, the position of corresponding lines differing only by the splitting between levels of equal K of the case (b) state. Often these satellites are not

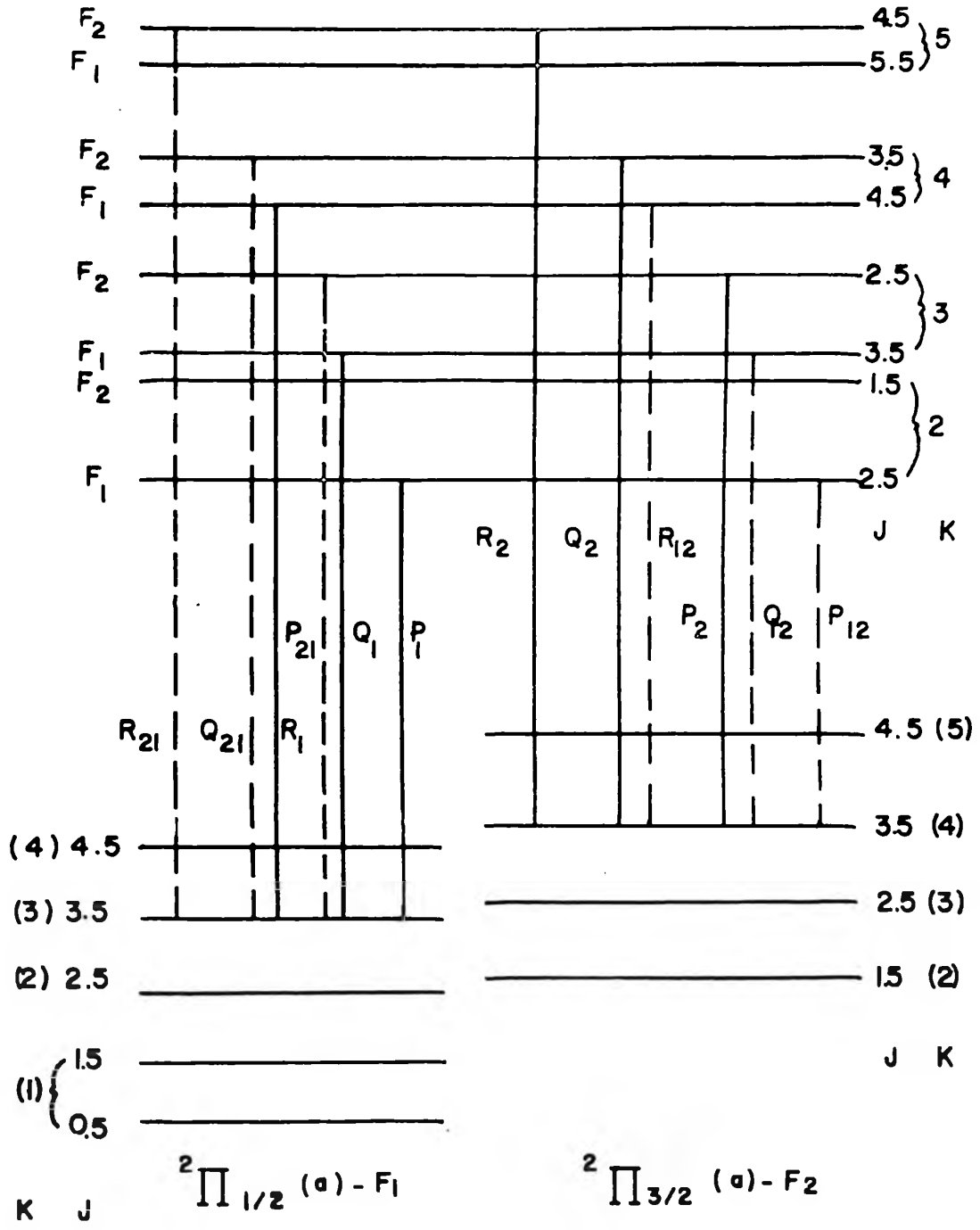

Fig. 15. The J'' = 3.5 Lines of the Twelve Branches of a $^2\Delta^{(b)} - {}^2\Pi^{(a)}_{ref}$ Transition. Satellite transitions are shown by broken lines. The order of the upper-state levels corresponds to $Y' \approx -6$.

separately resolved. The two satellite branches P_{12} and R_{21} have $\Delta K = \pm 2$ and are allowed only in (b) - (a) transitions. The intensities of the six satellite branches increase as the difference between the coupling in initial and final states becomes more marked. In the limit of a "pure case (b)" - "pure case (a)" transition, all twelve branches are equally intense.

Formulae are given in Appendix II for the frequencies of the lines in each of the twelve branches shown in Fig. 15. It is shown how, in a "pure case (b)" - case (a) transition, the lines follow parabolic formulae. In a "near case (b)" - case (a) transition, where the case (b) state shows tendencies towards case (a) coupling, the low-J lines of each branch deviate from parabolic formulae. These irregularities are called "low-J deviations" throughout this thesis.

The structure of a band can be illustrated by a Fortrat diagram, in which the frequencies of the lines are plotted against J for each branch. Four such diagrams are shown in Fig. 16. "Pure case (b)" - case (a) and "near case (b)" - case (a) transitions are illustrated in Figs. 16(a) and 16(b). Other types of transitions which might be expected in the CCl molecule are shown in Figs. 16(c) and 16(d). The bands illustrated in Fig. 16 are all degraded towards higher frequencies, indicating that the internuclear distance is greater in the lower than in the upper state. (See Appendix II). The directions in which the "low-J deviations" occur depend on the order of the energy levels of the case (b) state. The "low-J deviations" of Fig. 16(b) correspond to the order shown in Fig. 15.

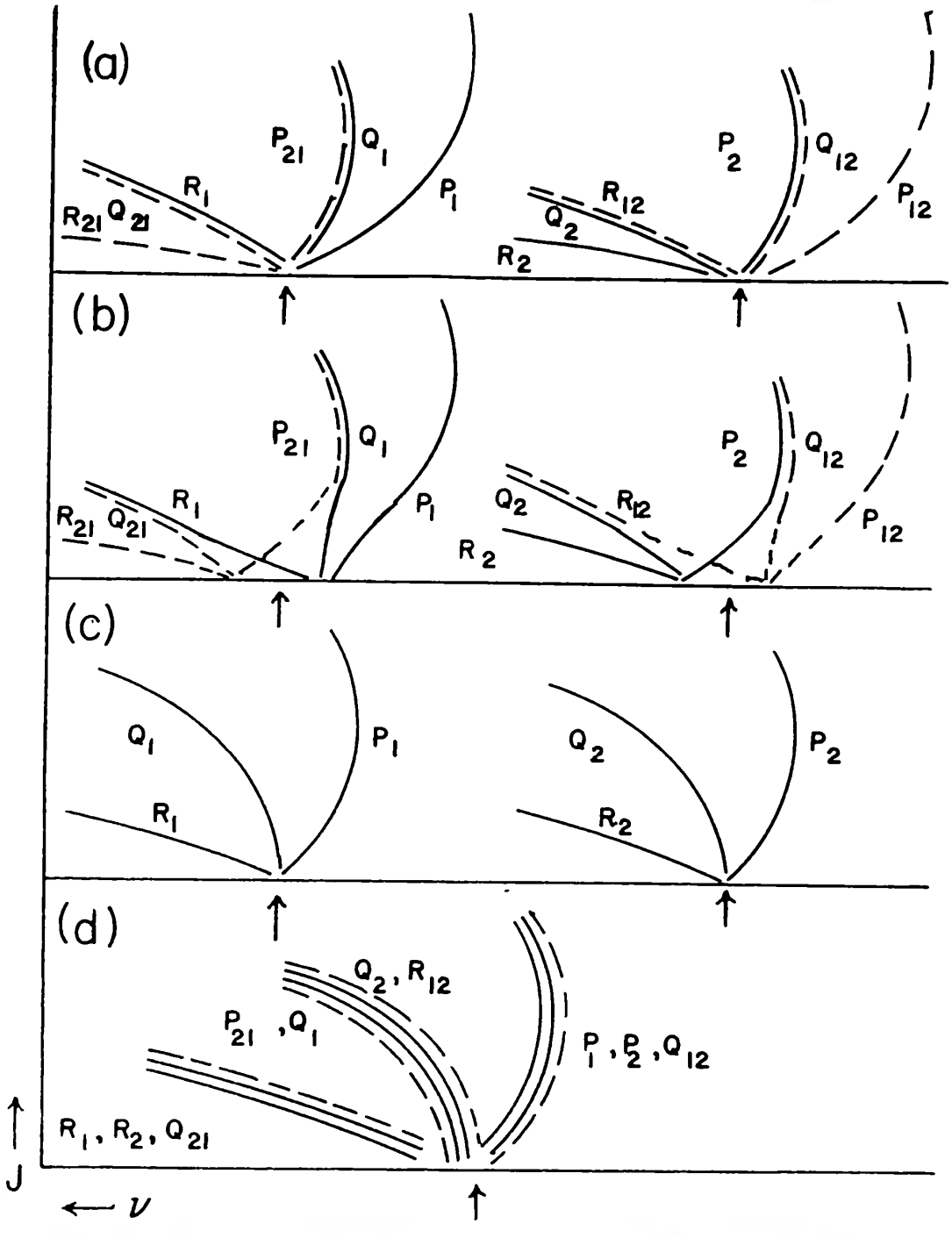

Fig. 16. Portrait Diagrams. (a) Pure case (b) - case (a); (b) Near case (b) - case (a); (c) Case (a) - case (a); (d) Case (b) - case (b). Main branches are shown by solid lines, and satellite branches by broken lines. Arrows indicate sub-band origins.

CHAPTER 8.

ROTATIONAL ANALYSIS OF THE 2780 A° BAND OF THE CCl MOLECULE

I. ASSIGNMENT OF THE TRANSITION:- As described in Chapter 6, the intense spectrum emitted at 2780 A° by a discharge in CCl_4 vapour was photographed under high resolution. A microdensitometer profile of the prominent band in this region is reproduced in Fig. 17. The simple double-headed structure of this band shows that the emitter is a diatomic or linear polyatomic molecule with an odd number of electrons. It may be assumed that this emitter contains chlorine, since the spectrum was excited in a number of chlorine-containing Freons, but not in chemically similar, chlorine-free Freons. The rotational constants obtained in the analysis below are consistent only with the CCl molecule being responsible for the spectrum.

The band in Fig. 17 consists of two sub-bands, separated by about 140 $cm.^{-1}$, with two prominent heads, labelled Q_1 and P_2, degraded to higher frequencies. Two other intensity maxima can be seen which are the heads of an underlying band. Within each sub-band, four intense branches can be picked out. They are labelled P_{12}, P_2, Q_2, R_2; P_1, Q_1, R_1, R_{21}. The presence of two widely separated sub-bands indicates that the transition involves a case (a) doublet state. The presence of a fourth intense branch in each sub-band indicates that the other state must have case (b) coupling. The eight intense branches listed above correspond to eight of the branches shown in Figs. 16(a), (b) for a doublet case (b) - doublet case (a) transition. A total of twelve

branches occur in such a transition, but as explained in Chapter 7, four of the satellite branches are not expected to be separately resolved. In Figs. 16(a), (b) the branches P_{12} and P_1 form heads at high values of J. No such heads appear in Fig. 17 because, at such high J values, the intensity of emission is very low.

The lines of the observed branches do not follow parabolic formulae at lower values of J. These "low-J deviations" indicate that the case (b) state has some tendency towards case (a) coupling, and therefore cannot be $^2\Sigma$. It can be seen from Fig. 17 that low J lines of the Q_2 branch are bunched together, giving a head-like appearance, while those of the corresponding R_1 branch are more widely spaced, and extend almost to the Q_1 head. The Q_2 branch is closely paralleled by its less intense satellite R_{12}, and most of the R_{12} lines are not separately resolved. Near the sub-band origin, however, the "low-J deviations" occur also in the head-forming branches Q_1 and P_2. Deviations in the latter are in such a direction as to diminish the spacings between lines, and none of the Q_1 lines are resolved. In the P_2 branch, the deviations tend to increase the line spacings, and a number of low-J lines are resolved. The low-J effects described above are the same as those predicted in Fig. 16(b). In section IV below, these effects are considered quantitatively when the separation $\delta'(K)$ between the two case (b) sub-states is determined.

Two of the intense observed branches are of Q type, with $\Delta J = 0$. The Q_2 branch is distinct from its satellite R_{12} at low J values, and Q_2 lines appear strongly between the more widely spaced R_2 lines. The high intensity of the head in the Q_1 branch cannot be ascribed to the accompanying satellite branch P_{21}, since it can be calculated that the

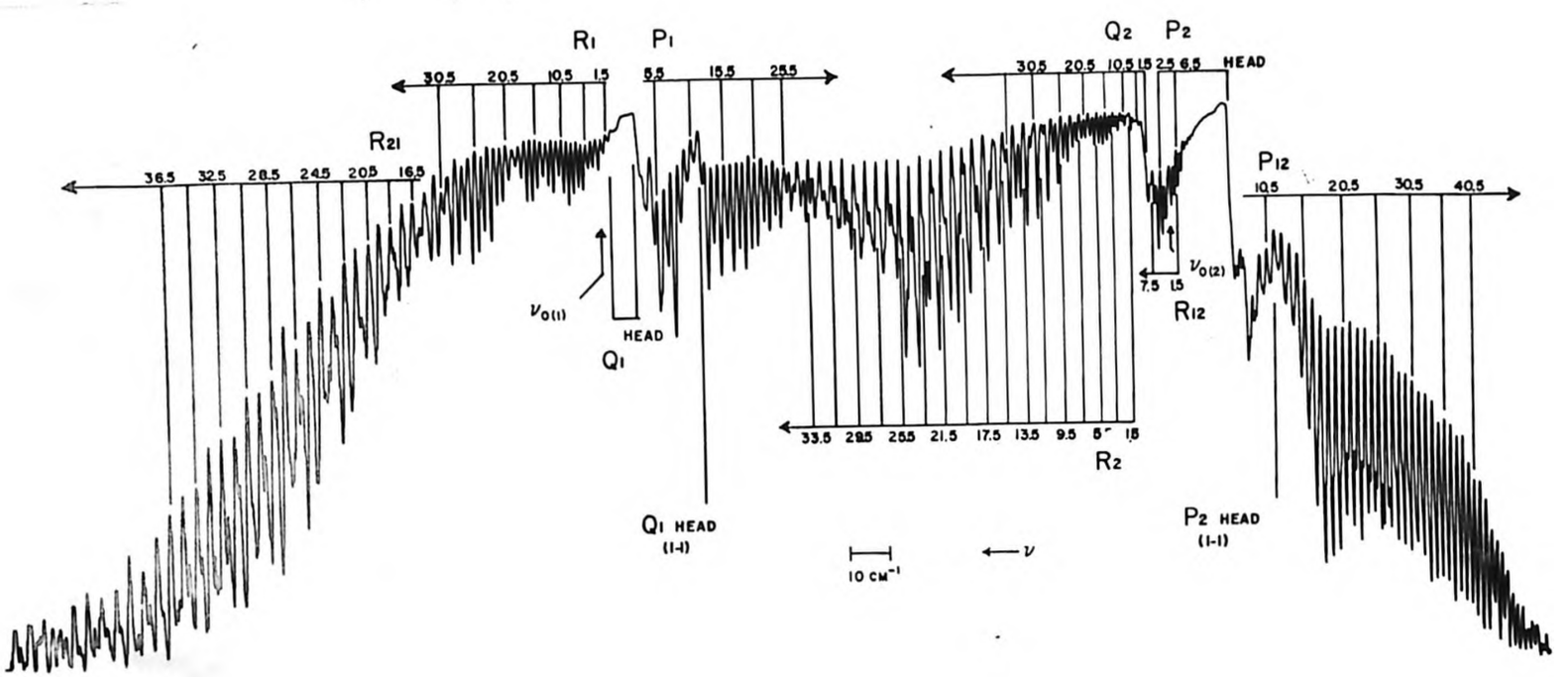

Fig. 17. A Microdensitometer Trace of the CCl Spectrum at 2700 A°, Under High Resolution.

latter would form a head 1 cm.$^{-1}$ to lower frequencies, and such a head does not appear with appreciable intensity. It follows that $\Delta \Lambda = \pm 1$ for the transition.

The electron configuration of CCl requires a $^2\Pi_{reg}$ ground state. Electronically similar molecules, such as SiF,[54] CF,[55] and NO,[57] all have $^2\Pi_{reg}$ case (a) lower states for transitions observed under similar experimental conditions. If it is assumed that the lower state of CCl is also of this type, the observed transition must be $^2\Delta$ case (b)-$^2\Pi_{reg}$ case(a). This assignment is confirmed by the Λ-type doubling effects described in Section VII below. In Section IV it is shown that the $^2\Delta$ state is inverted.

In their rotational analysis, Kuzyakov and Tatevskyi[31] assigned the CCl spectrum to a $^2\Sigma - ^2\Pi$ transition. The evidence presented above for a $^2\Delta$ upper state depends on a comparison of the spacings of low-J lines in corresponding branches of the two sub-bands. Significantly, Kuzyakov and Tatevskyi analyzed only one of the sub-bands. In the analysis described in this chapter both sub-bands were used, and all attempts to analyze the spectrum in terms of a $^2\Sigma - ^2\Pi$ transition failed.

II. <u>THE COMBINATION PRINCIPLE</u>:- The frequencies of all the observed lines are listed in Appendix III. The remainder of this analysis is based on six branches, P_{12}, Q_2, R_2, P_1, R_1, and R_{21}, in each of which a large number of lines were resolved.

In principle the rotational constants of the two states could be determined by fitting the observed line frequencies to the formulae for the branches given in Appendix II. In practice it is more convenient to use the combination principle. Relations called combination

differences are set up in which the difference in energy of two rotational levels of the same vibronic state is expressed as the difference in frequency of two lines of different branches. The combination differences used in this analysis are given in equations (10) to (14). They can be derived from the formulae for the branches in Appendix II. The necessary energy level expressions are derived in Appendix I from the general Hill and Van Vleck expression [equation (7) of Chapter 7]. All approximations made are justified in Appendix I.

To use the combination differences, it is necessary to know the correct numbering of the lines in each branch. In most spectra this numbering is determined readily by inspection. The origin of each subband is indicated by a central gap, corresponding to certain missing lines, and the numbering begins at that origin. In the CCl spectrum, the "low-J deviations" obscure the central gaps, and the numbering must be determined by other means.

III. LOWER STATE CONSTANTS AND NUMBERING OF THE LINES:- Equation (10) and (11) below give the effective rotational constants, $(B_{eff})_i''$, of the $^2\Pi_{3/2}$ and $^2\Pi_{\frac{1}{2}}$ sub-states respectively.*

$$R_2(J-1) - Q_2(J) = F_2''(J) - F_2''(J-1) = 2(B_{eff})_2''J. \qquad (10)$$

$$R_1(J-1) - P_1(J+1) = F_1''(J+1) - F_1''(J-1) = 4(B_{eff})_1'' (J+\tfrac{1}{2}). \qquad (11)$$

These combination differences, if evaluated from correctly numbered lines, involve only separations between lower-state rotational levels. If they are evaluated from incorrectly numbered lines, the resulting expressions

*The superscripts ' and '' denote upper and lower-state quantities respectively. The introduction of effective rotational constants is explained in Appendix I.

are then functions of the levels of both electronic states, and do not have the analytical form given by equations (10) and (11). Such incorrectly evaluated expressions do not vanish for $J=0$ or $(J+\frac{1}{2})=0$ respectively, and are not quite linear in J. The non-linearity is due to the inclusion of the quantity H(J), which is defined in Appendix I. H(J) occurs in the upper-state energy level expressions, and accounts for the tendencies of that case(b) state towards case (a) coupling. To a first approximation, H(J) is inversely proportional to $(J+\frac{1}{2})$. It is cancelled only if equations (10) and (11) are evaluated from correctly numbered lines.

The numberings of the four branches which appear in the above combination differences were varied systematically. For each numbering scheme the combination differences were evaluated and fitted to a linear expression by the method of least squares.*

The results of this procedure are given in Table 5. The constant and linear coefficients, a_0 and a_1 respectively, of the least-squares equations are given in the fourth and fifth columns. As shown above, a_0 is expected to vanish if, and only if, the numbering of the lines is correct. The quantity V is the sum of the squares of the residuals obtained from the least-squares treatment. It is a measure of how well

*The combination differences for each value of J were fitted to the power series $y(x) = a_0 + a_1x + a_2x^2 \ldots$, where $x = J$ or $(J+\frac{1}{2})$. The coefficients a_j and their standard deviations were calculated according to the least-squares method of Birge.[58] In Appendix I, centrifugal stretching terms and certain other contributions to rotational energy were neglected. These contributions would have appeared in equations (10), (11), and (13) as quadratic or higher coefficients of x. In the fitting of these equations, with the correct numbering, quadratic and higher coefficients were smaller than the standard deviations of the linear coefficients. This is further justification for the approximations of Appendix I.

TABLE 5.

RESULTS OBTAINED FROM EQUATIONS 10 AND 11 WITH VARIOUS NUMBERING SCHEMES

The numbering schemes are indicated in the first two columns by the frequencies of the lines whose assignments are indicated. The correct schemes are marked #. The errors quoted are standard deviations. Only for the numbering schemes marked # are the coefficients a_0 less than their standard deviations.

Combination Difference (10): Evaluated from J = 4.5 to 33.5.

$$R_2(J-1) - Q_2(J) = 2(B_{eff})_2'' = a_0 + a_1 J.$$

$R_2(9.5)$	$Q_2(9.5)$	V	a_0	a_1
35890.49 cm.$^{-1}$	35875.36 cm.$^{-1}$	0.982	-0.155 cm.$^{-1}$	
35892.79	35875.95	0.575	0.879	
35892.79	35876.64	0.349	0.440	
35892.79#	35877.37	0.231	(-0.005 $\pm$0.08)	(1.39012 $\pm$0.00192) cm.$^{-1}$
35892.79	35878.13	0.257	-0.517	
35894.97	35878.94	0.354	0.321	

Combination Difference (11): Evaluated from J = 5.5 to 27.5.

$$R_1(J-1) - P_1(J+1) = 4(B_{eff})_1'' (J+\tfrac{1}{2}) = a_0 + a_1 J.$$

$P_1(9.5)$	$R_1(9.5)$	V	a_0	a_1
36007.01 cm.$^{-1}$	36010.50 cm.$^{-1}$	0.821	-0.881 cm.$^{-1}$	2.80158 cm.$^{-1}$
35981.04	36009.30	0.231	1.02	2.77324
35981.04#	36008.12	0.296	(0.026 $\pm$0.04)	(2.75569 $\pm$0.00404)
35981.04	36007.01	0.249	-0.992	2.73648

the observed data fits a linear equation. For the correct numbering scheme, with which the non-linear term H(J) is cancelled, V is expected to be a minimum.

For the correct numbering of the Q_2 and R_2 branches, V is a minimum, and a_0 of equation (10) vanishes, as predicted. The correct numbering of the R_1 and P_1 branches was taken to be that for which a_0 of equation (11) vanished, although V is not a minimum for this numbering. The magnitude of V, however, is not as sensitive a criterion of non-linearity in equation (11) as it is in equation (10) where the slope is only half as great. The numbering of the R_1 and P_1 branches was confirmed by an additional test. Approximate values of B" and (Y"-2) quoted in Appendix I can be used to show that $(B_{eff})_1" = (0.99 \pm 0.002) \times (B_{eff})_2"$, from which it follows that the linear coefficient a_{-1} of equation (11) should fall within the limits (2.7524 ± 0.0056) cm. This condition is met only for the numbering scheme already taken to be correct.

The effective rotational constants $(B_{eff})_i"$ were obtained from the coefficients a_1. The true rotational constant $B_0"$ is the mean of the two effective rotational constants, and is given in Table 6.*

Two independent combination differences give the separation of the sub-states $^2\Pi_{3/2}$ and $^2\Pi_{\frac{1}{2}}$, as shown in equation (12).

$$\delta"(J) = P_1(J) - P_{12}(J) = R_{21}(J) - R_2(J) = F_2"(J) - F_1"(J)$$
$$= B_0"(Y"-2) + \left[(B_{eff})_2" - (B_{eff})_1"\right] \quad J(J+1) \qquad (12)$$

*The band on which this rotational analysis is being performed is shown in Chapter 9 to be the (0-0) band of the system. The subscript v, in the symbols for the rotational constants, is thus 0.

The numbering of the P_1 and R_2 branches is known from above. For a unique numbering of the P_{12} and R_{21} branches, the two combination differences above agreed for all values of J. The numbering of all six branches used in the analysis was therefore determined.

The combination differences of equation (12) were evaluated over the range $J = 6.5 - 34.5$, and the following least-squares equation was obtained:

$$\delta''(J) = (133.57 \pm 0.13) + J(0.0158 \pm 0.0142) + J^2(0.00635 \pm 0.0035) \text{ cm.}^{-1} \qquad (12a)$$

The constants B" and A" were calculated from the constant term, and are quoted in Table 6. Within the standard deviations given, the coefficients of J and J^2 in equation (12a) give the value $[(B_{eff})_2'' - (B_{eff})_1''] = 0.006 \text{ cm.}^{-1}$ obtained from combination differences (10) and (11).

IV. UPPER STATE CONSTANTS.- The following combination difference gives B_0', the upper-state rotational constant, independently of the quantity H(J):

$$\begin{aligned} R_1(J) - P_1(J) + R_2(J) + R_2(J-1) - Q_2(J) - Q_2(J-1) \\ = [P_1'(J+1) + P_2'(J+1)] - [P_1'(J-1) \quad P_2'(J-1)] \\ = 4B_0' \ (J+\tfrac{1}{2}). \end{aligned} \qquad (13)$$

It was evaluated from $J = 4.5$ to 26.5, and a least-squares treatment gave the value of B_0' quoted in Table 6.

The combination difference below gives the separation of levels of equal K in the $^2\Delta$ state.

$$\begin{aligned} \delta'(K) = P_2'(K) - P_1'(K) = \delta''(J) - [R_1(J) - Q_2(J)] \\ = B_0'\left[\sqrt{K^2+\alpha} + \sqrt{(K+1)^2+\alpha} - (2K+1)\right] \end{aligned} \qquad (14)$$

where $\alpha = Y'(Y'-4) \Lambda^2/4$. J and K are lower and upper-state quantum numbers respectively. It can be verified from Fig. 15 of Chapter 7 that $K = J + \frac{1}{2}$.

This combination difference was evaluated using the Δ'' values of the least-square equation (12a). A computer programme was set up to give the difference between observed values of Δ', and values calculated using an arbitrary α, for each value of K from 2 to 24. A minimum residual deviation of 0.139 cm.$^{-1}$ was obtained for $\alpha = 57.98$.*

It follows from the discussion in Appendix II that equation (14) is valid for the ($J' = 1.5$, $K' = 2$) level of the $^2\Delta$ state only if that state is inverted (i.e. $Y' < 2$). If $Y' > 2$, this anomalous level is described by the F_1' rather than by the F_2' energy expression. For a regular $^2\Delta$ state (i.e. $Y' \geq 2$) the frequencies of the lines originating from this level do not obey the general formulae given in Table 9 of Appendix II, but are shifted to lower frequencies. $\Delta'(K = 2)$ is decreased by the same amount. The shift is given by $F_1'(J' = 1.5) - F_2'(J' = 1.5) = -2B_0'(4+\alpha)^{\frac{1}{2}} = -11.1$ cm.$^{-1}$ Of the five lines which involve the anomalous level, only two, $P_2(2.5)$ and $Q_2(1.5)$, were resolved. These lines do obey the general formulae of Appendix II, and there is no evidence of a shift of 11.1 cm.$^{-1}$ to lower frequencies. It may therefore be concluded that the $^2\Delta$ state is inverted. Of the two values of Y' which are roots of $Y'(Y'-4)\Lambda^2/4 = \alpha = 57.98$, the one satisfying the condition $Y' < 2$ was taken and is given in Table 6.

V. ORIGINS OF THE SUB-BANDS: The origin $\nu_0(2)$ of the $^2\Delta - {}^2\Pi_{3/2}$ sub-band was determined from a least-squares treatment of the following combination relation:

---

*In equation (14), a term $-\gamma(K+1)$ should have been added to account for spin splitting. Compare equation (14) and equation (30) of Appendix I. This effect, however, is not expected to be large for a Δ state. If the term in γ is significant, it would be expected that the differences between observed and calculated values of Δ' would vary linearly with K. These differences were found to be quite random; thus the neglect of the term in γ is justified.

TABLE 6.

ROTATIONAL CONSTANTS FOR THE (0-0) BAND OF THE CCl SPECTRUM

Errors are quoted as standard deviations.

Upper $^2\Delta_{inv}$ case (b) State:

$T_0'(v' = 0) = \nu_0(1) = 36{,}000.92 \pm 0.25$ cm.$^{-1}$

$B_0' = 0.70533 \pm 0.00062$ cm.$^{-1}$

$r_0' = 1.63546 \pm 0.00073$ A°

Doublet Splitting: $Y' = -5.87$

$A' = B_0'Y' = -4.14$ cm.$^{-1}$

Lower $^2\Pi_{reg}$ case (a) State:

$T_0''(^2\Pi_{3/2}, v'' = 0) = B_0''(Y''-2) = 133.57 \pm 0.13$ cm.$^{-1}$

$T_0''(^2\Pi_{\frac{1}{2}}, v'' = 0) = 0$ cm.$^{-1}$

$(B_{eff})_1'' = 0.68692 \pm 0.00101$ cm.$^{-1}$

$(B_{eff})_2'' = 0.69506 \pm 0.00096$ cm.$^{-1}$

$B_0'' = 0.69199 \pm 0.00069$ cm.$^{-1}$

$r_0'' = 1.65115 \pm 0.00081$ A°

Doublet Splitting: $Y'' = 195.03 \pm 0.19$

$A'' = B_0''Y'' = 134.96 \pm 0.13$ cm.$^{-1}$

Sub-band Origins:

$\nu_0(1) = 36{,}000.92 \pm 0.25$ cm.$^{-1}$

$\nu_0(2) = 35{,}867.35 \pm 0.12$ cm.$^{-1}$

$$R_2(J-1) + P_{12}(J+1) = 2\nu_0(2) + B_0'/2 - 2(B_{eff})_2'' \quad 2J(J+1)\left[B_0' - (B_{eff})_2''\right] . \qquad (15)$$

It was not possible to use a similar relation to determine $\nu_0(1)$, since lines, close to that origin , were not resolved, and serious errors of extrapolation would be introduced. Greater precision was obtained using the relation

$$\nu_0(1) = \nu_0(2) + B_0''\ (Y'' - 2) \qquad (16)$$

which follows from the definitions of the origins in Appendix II.

VI. SUMMARY OF MEASURED QUANTITIES FOR THE 2780 A° BAND:- The results of the rotational analysis are given in Table 6.

The quantities T_0 are the energies of the vibronic states, referred to $^2\Pi_{\frac{1}{2}}$ $(v'' = 0)$ as zero. The distinction between vibronic and rotational energy, which is necessarily arbitrary, is described in Appendix I.

The internuclear distances r_v in each state are obtained from the rotational constants by the relation

$$r_v = (h/8\pi^2 c \mu B_v)^{\frac{1}{2}} \qquad (17)$$

where μ is the reduced mass of the atoms. In calculating μ it is assumed that the emitter is the species $C^{12}Cl^{35}$.

The constants D_v were too small to measure accurately. As shown in Appendix I, they are of the order of 2×10^{-6} cm.$^{-1}$ in each state.

As a check on the analysis, the frequencies of all the observed lines were calculated from the formulae of Appendix II and the constants given in Table 6. The observed and calculated frequencies agreed within the limits set by the accuracy of measurement of the lines.

VII. FINE STRUCTURE: Many of the lines listed in Appendix III could be resolved into two or more closely-spaced components. Lines of the

$^2\Delta - {}^2\Pi_{3/2}$ sub-band have two components, a and b, as shown in Fig. 18(a). The separation of these components does not vary with J, within the limits of observation, and amounts to about 0.27 cm.$^{-1}$ Lines of the $^2\Delta - {}^2\Pi_{\frac{1}{2}}$ sub-band have three components, d, e, and f, as shown in Fig. 18(b). The separation of the outer two components, d and f, increases linearly with J, varying from about 0.3 cm.$^{-1}$ at very low J to about 0.7 cm.$^{-1}$ at J = 30.5.

The occurence of three components in the $^2\Delta - {}^2\Pi_{\frac{1}{2}}$ sub-band, and the constant separation of the two components in the other sub-band, are not consistent with Λ-type doubling effects, as described in Chapter 7. It was therefore assumed that the two components in the $^2\Delta - {}^2\Pi_{3/2}$ sub-band arose from some other effect. Λ-type doubling is not expected to be appreciable in this sub-band. The fine structure of the $^2\Delta - {}^2\Pi_{\frac{1}{2}}$ sub-band was assumed to result from a superposition of the doubling described above and Λ-type doubling. The four components thus expected were only resolved into three, with the centre one being more intense. The observed linear increase with J of the total line width is that expected for the appreciable Λ-type doubling in a $^2\Pi_{\frac{1}{2}}$ sub-state. The relative magnitude of the Λ-type doubling in the two sub-bands serves to confirm the assignment of the transition made in Section I.

In the first kind of doubling (i.e. the kind not attributed to Λ-type doubling), the second component cannot be one of the satellite lines which closely parallel lines of the main branches, since this doubling appears in the P_{12} and P_1 branches which have no accompanying satellites. Neither is the second component likely to be a line of the CCl^{37} molecule, since the spectrum of this isotopic species would be

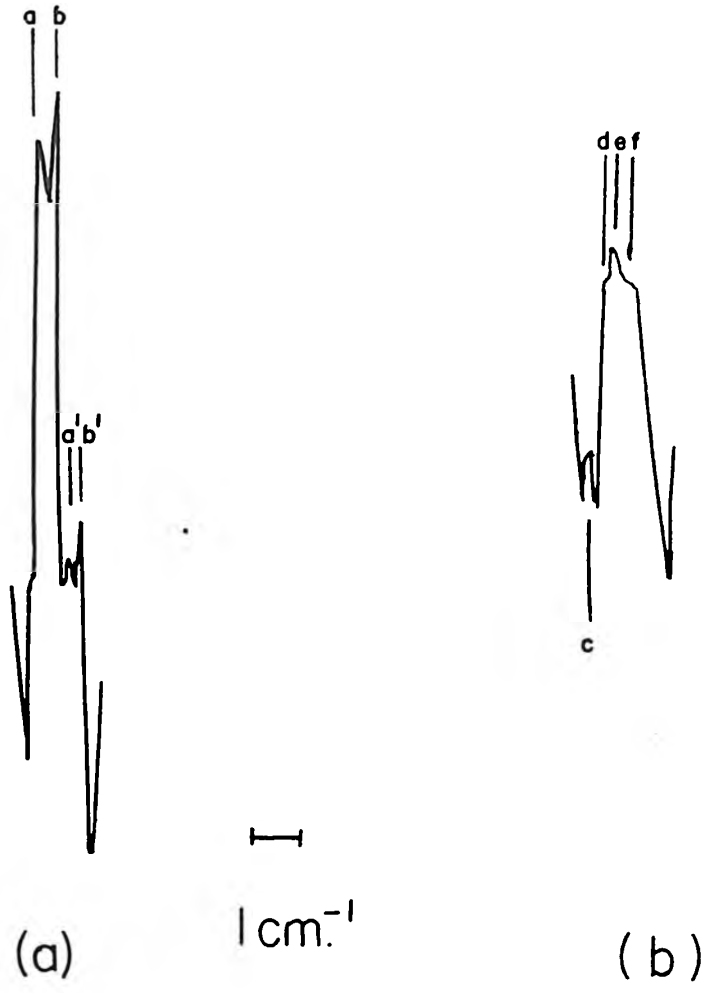

Fig. 18. Fine Structure. (a) Doubling in $P_{12}(20.5)$; (b) Tripling in P_1 (15.5).

only a third as intense as that of the more abundant CCl^{35}. Also, the separation of lines due to two isotopic species does not remain constant with increasing J. The small peaks a', b', and c in Fig. 18 probably are lines of the CCl^{37} spectrum. Again, since they appear in the P_{12} and P_1 branches, they cannot be satellite lines. No analysis of these isotopic lines was attempted, since they appear on the original spectrogram in very poor contrast, and cannot be measured accurately.

The doubling may possibly be a spurious effect, arising from faulty spectroscopic technique. In such a case, however, a broadening of the lines, rather than a splitting into two components, would be expected. In Chapter 6 it is described how temperature and pressure effects, which might cause such a broadening, were investigated and found to be negligible.

A Zeeman effect, caused by the magnetic field of the microwave radiation, may have caused the doubling. In case (a) states, the magnetic moment in the direction of $\underline{J}$ is space-quantised, and each rotational level is split into $2J+1$ components by an external magnetic field. The total width of the multiplet decreases in inverse proportion to $(J+1)$, and for high values of J the splitting is negligible. In case (b) states, the angular momenta associated with $\underline{S}$ and $\underline{K}$ are often uncoupled by external magnetic fields, and each is independently space-quantized. Each rotational level is split into two components, corresponding to different orientations of $\underline{S}$ to the external field. Each of these components is further split into $2K+1$ components, corresponding to different orientations of $\underline{K}$. The latter splitting, however, is negligible at high K, as is the splitting of each J level,

in case (a).[47] In CCl, each rotational level of the case (b) state would thus be split effectively into two components, with a separation independent of J and of K. No appreciable splitting would occur in the case (a) state except at very low J. The doubling of the lines would therefore be explained.

The doubling could also be attributed to quadrupole interactions of the chlorine nucleus.[47] The observed doubling, however, is very small, of the order of the resolution , and only speculative conclusions may be made as to its origin.

CHAPTER 9.

VIBRATIONAL ANALYSIS OF THE CCl SPECTRUM

A microdensitometer profile of the entire observed CCl spectrum is shown in Fig. 19. It was taken from a low-resolution spectrogram, similar to Fig. 3, but more heavily exposed in order to bring out the weaker features. A second microdensitometer profile, in Fig. 20, shows under high resolution the band heads in the 2850 A° region. The frequencies and vibrational assignments of the observed band heads are given in Table.7.

According to the rotational analysis, each band in this system may be identified by a Q_1 and a P_2 head, separated by about 140 $cm.^{-1}$ In calculating the positions of the vibrational energy levels, the frequencies of the sub-band origins, rather than the frequencies of the heads, should be used. The exact head-origin separation in a given band, however, can be determined only from a rotational analysis of that band. Since this was done for only one band, the frequency of each band is taken to be the mean of the frequencies of its Q_1 and P_2 heads. The separation of these two heads is almost equal to the separation of the corresponding sub-band origins.

The identification of the Q_1 and P_2 heads in each band is complicated by the head-like appearance of the low-J lines of the Q_2 branch. A comparison of Figs. 18 and 19(b), which are high and low-resolution profiles respectively of the same part of the spectrum, shows how the intensity maximum labelled $Q_2(0\text{-}0)$ could easily be mistaken for a true

head, indicating the presence of an additional band.

Previous vibrational analyses of the CCl spectrum[24,27-31] were made under lower resolution than was used in the work described in this thesis. The "low-J deviations" which cause the appearance of a spurious Q_2 head were not recognized, and incorrect assignments of the bands resulted. Also, the two closely-spaced bands at 2850 A° , labelled (0-1) and (1-2) in Fig. 20, were not separately resolved. For these reasons, the new vibrational analysis described in this chapter was necessary.

The energies of the vibrational levels of each electronic state are given by[47]

$$G(v) = \omega_e(v+\tfrac{1}{2}) - \omega_e x_e (v+\tfrac{1}{2})^2 + \ldots \qquad (18)$$

where v is the vibrational quantum number. The constants ω_e and $\omega_e x_e$ are the vibrational frequency and the anharmonicity constant respectively, both referred to the minimum of the vibrational potential curve. $\omega_e \gg \omega_e x_e > 0$. To a first approximation, the vibrational levels are equally spaced, with a separation ω_e. Terms in quadratic and higher powers of $(v+\frac{1}{2})$ account for the fact that higher vibrational levels become more closely spaced, because of the anharmonic nature of the vibrational potential curve.

A given band is designated by the upper and lower-state quantum numbers, v' and v" respectively, of the vibrational levels involved in the transition. For example, the designation (0-1) indicates that $v' = 0$ and $v'' = 1$. A series of bands in a given system for which $\Delta v = (v' - v'')$ is constant is called a sequence. The separation between different sequences is of the order of ω_e, while the separation between the bands within a given sequence is much smaller, of the order of $(\omega_e' - \omega_e'')$.

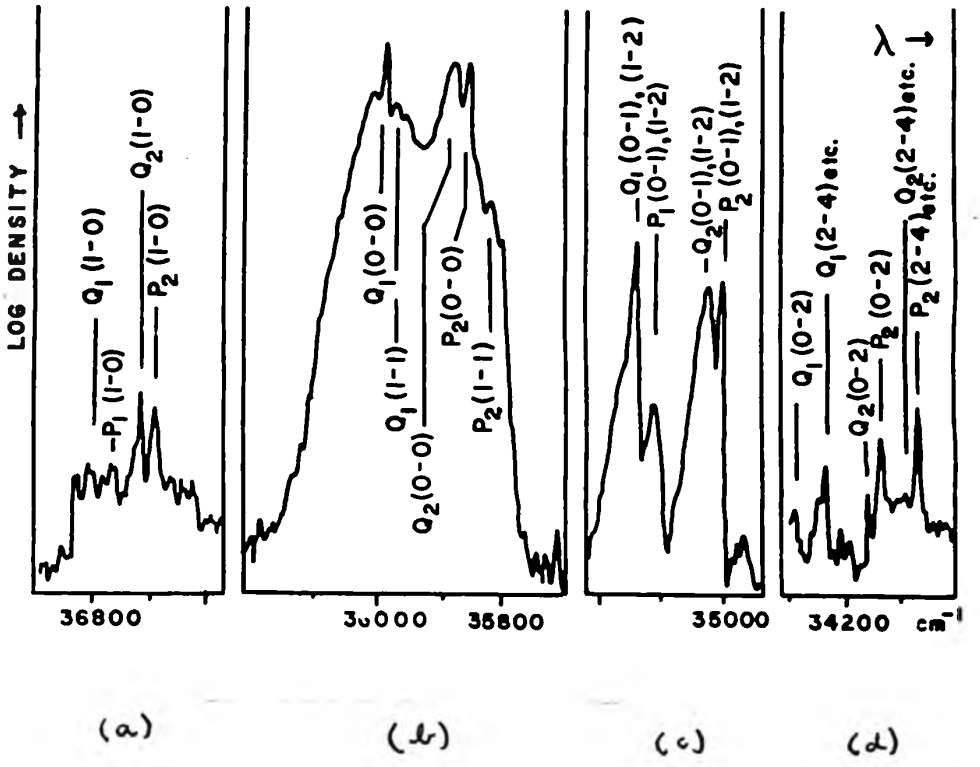

Fig. 19. Microdensitometer Traces of the CCl Spectrum at (a) 2714, (b) 2780, (c) 2850, and (d) 2920 A°.

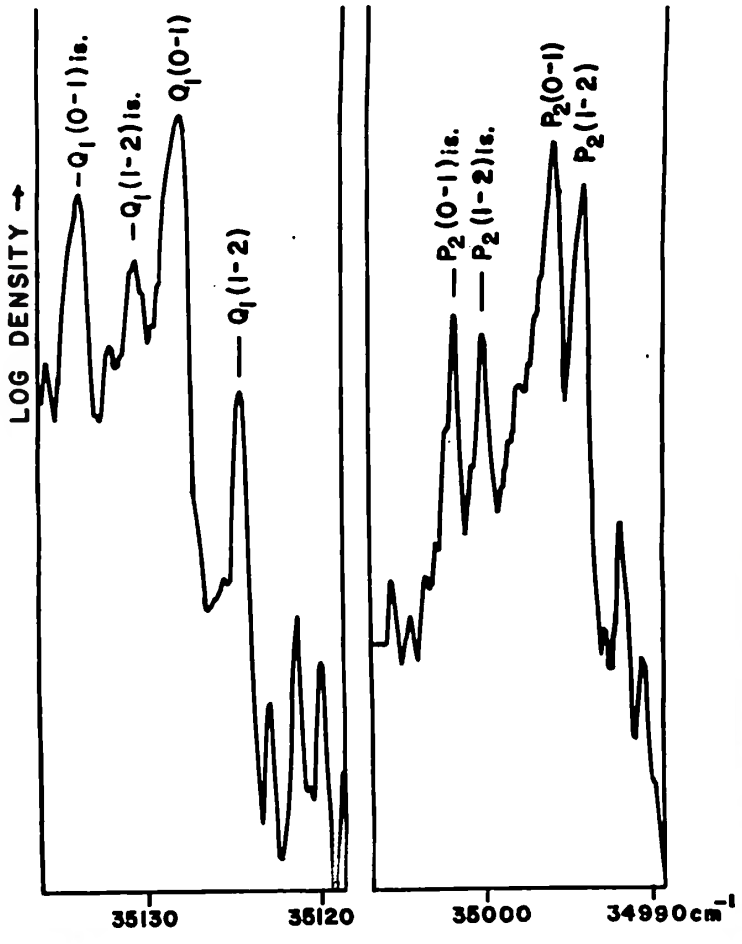

Fig. 20. A High-Resolution Microdensitometer Trace of the CCl Band Heads at 2850 A°.

TABLE 7.

FREQUENCIES AND ASSIGNMENTS OF BAND HEADS AND BANDS

Sequence	Head Frequency		Doublet Separation	Band Frequency	
	Q_1	P_2	Q_1-P_2	$(Q_1+P_2)/2$	
$\Delta v = 1$ (2714 A°)	36836	36700	136	36768	(1-0)
$\Delta v = 0$ (2780 A°)	35992.2	35854.1	138.1	35923.1	(0-0)
	976.3	837.8	138.5	907.1	(1-1)
$\Delta v = -1$ (2850 A°)	35134.2	35001.8	132.4	35068.0	(0-1)i
	130.9	000.1	130.8	65.4	(1-2)i
	128.2	34995.7	132.5	61.9	(0-1)
	124.6	993.9	130.7	59.2	(1-2)
$\Delta v = -2$ (2920 A°)	34284	34147	137	34215	(0-2)
	34246	34098	148	34172	(2-4), etc.

Frequencies are given in $cm.^{-1}$ Bands of CCl^{37} are designated by the symbol i.

The spectrum in Fig. 19 consists of four clusters of bands, separated by approximately equal intervals of 860 cm.$^{-1}$ The bands within each cluster form a sequence. Since the internuclear distances in the upper and lower electronic states differ by only 1%, it was assumed initially in accordance with the Franck-Condon principle, that the most intense bands, occuring at 2780 A° , form the $\Delta v = (v' - v'') = 0$ sequence. The bands at 2714, 2850, and 2920 A° are thus the $\Delta v = 1$, -1, and -2 sequences respectively.

According to empirical rules stated by Herzberg,[47] the vibrational frequencies, ω' and ω'' in the upper and lower states respectively do not differ greatly if the corresponding internuclear distances are not very different. The separation between the sequences indicates that both vibrational frequencies are of the order of 860 cm.$^{-1}$

Bands due to CCl^{37} are expected to appear with appreciable intensity, and with nearly the same separation of Q_1 and P_2 heads found in the more intense CCl^{35} bands. The frequency shift between bands of the two isotopic molecules may be calculated from the approximate vibrational frequencies given above. A negligible shift is expected in the $\Delta v = 0$ sequence. In the $\Delta v = -1$ sequence, an interval of 6 cm.$^{-1}$ is expected between band heads of the two molecules, with the CCl^{37} heads at higher frequencies. Appreciable shifts are expected in the other two sequences, but as the intensity of these sequences is so low, it is unlikely that CCl^{37} bands would be observed.

The isotopic shifts predicted above for the various sequences were observed. Heads due to CCl^{37} are shown in Fig. 20. The shifts in the bands labelled (0-1) and (1-2), both members of the $\Delta v = -1$ sequence, are 6.1 and 6.2 cm.$^{-1}$ respectively. In the $\Delta v = 0$ sequence

at 2780 A°, where a negligible shift is predicted, no CCl^{37} heads are observed, as they lie beneath the intense CCl^{35} heads. The observed isotope effect confirms the assignment of sequences made above.

Under the experimental conditions used, electronically excited molecules undergo collisions, even during their short mean lifetime ($\gtrsim 10^{-8}$ seconds)[47] in the upper electronic state. These collisions tend to restore a Boltzmann energy distribution by removing the excess vibrational energy of the electronically excited molecules. Thus, almost all the electronic transitions responsible for the observed spectrum originate from the few lowest vibrational levels of the upper electronic state.

The two intense pairs of heads observed at 2780 A° thus belong to the (0-0) and (1-1) bands, and the two pairs at 2850 A° belong to the (0-1) and (1-2) bands. Which pair of heads in each sequence belongs to which of the two expected bands for that sequence is not immediately apparent.

Equation (18) can be used to show that

$$[(0\text{-}0) - (1\text{-}1)] - [(0\text{-}1) - (1\text{-}2)] = 2\,\omega_e''x_e'' > 0. \qquad (19)$$

The separation of the $\Delta v=0$ sequence bands is 16.0 $cm.^{-1}$, while the separation of the $\Delta v=-1$ sequence bands is only 2.7 $cm.^{-1}$ It follows that equation (19) is satisfied only if the higher-frequency band at 2780 A° is (0-0), and the lower-frequency band in the same sequence is (1-1). The (0-0) band is the most intense of the entire system, as would be expected from the Franck-Condon principle and from the arguments above.

Equation (20) predicts the frequency of the (1-0) band.

$$(1\text{-}0) = (1\text{-}1) + (0\text{-}0) - (0\text{-}1)$$

$$\approx \left\{ \begin{array}{l} 36{,}768.3 \text{ cm.}^{-1} \text{ if } (0\text{-}1) = 35{,}061.9 \text{ cm.}^{-1} \\ 36{,}771.0 \text{ cm.}^{-1} \text{ if } (0\text{-}1) = 35{,}059.2 \text{ cm.}^{-1} \end{array} \right\}. \qquad (20)$$

Two frequencies are given, since it has not yet been determined which of the two bands at 2850 A° is the (0-1) band. A band was observed at 2714 A°, with a frequency of 36,768 cm.$^{-1}$ There was no evidence of a band at the alternative frequency of 36,771 cm.$^{-1}$ The band at 36,768 cm.$^{-1}$ may thus be assigned to the (1-0) transiton. The assignment of the two $\Delta v = -1$ sequence bands at 2850 A° follows from the agreement between the first frequency (36,768.3) cm.$^{-1}$ calculated above for the (0-1) band, and the frequency actually observed for this band.

The predicted frequency of the (0-2) band is

$$(0\text{-}2) = (1\text{-}2) + (0\text{-}1) - (1\text{-}1) = 34{,}214.0 \text{ cm.}^{-1} \qquad (21)$$

The 2920 A° band is weak and complex, and its features cannot be identified with certainty; nevertheless, a pair of heads is observed, as shown in Fig. 19 with a mean frequency of 34,215 cm.$^{-1}$

The bands identified thus far involve the $v'' = 0$, 1, and 2 levels of the lower state, and the $v' = 0$, and 1 levels of the upper state. Their frequencies give the lower-state vibrational constants of Table 8, as well as a value of 845 cm.$^{-1}$ for the separation of the first two upper-state vibrational levels.

Two peaks at 2714 A°, yet unidentified, appear at 34,246 and 34,098 cm.$^{-1}$ They have the correct separation for a Q_1 and a P_2 head, but cannot be assigned to the (1-3) band, since they are more intense than the heads of the (0-2) band already identified. Also, this assignment would give 887 cm.$^{-1}$ for the separation of the $v'' = 3$ and $v'' = 2$

lower-state levels, implying negative anharmonicity. However, if $\omega_e' x_e'$ is given the plausible value of about 7.5 cm.$^{-1}$, it can be shown that the heads in successive bands of the $\Delta v = -2$ sequence will themselves converge at the observed head frequencies, and that this type of convergence will not occur for successive bands in other sequences. This accounts for the relatively high intensities of the two heads labelled (2-4) etc. in Fig. 19, and is consistent with the rest of the vibrational scheme.

The results of the vibrational analysis are given in Table 8. The quantities D_e are the dissociation energies of each electronic state, measured from the minimum of the potential curve. They are calculated from the following extrapolation formula:

$$D_e = \omega_e^2/4\,\omega_e x_e \,. \qquad (22)$$

This extrapolation is based on the assumption that the energies of all the vibrational levels are given exactly by equation (18), without the addition of terms in cubic or higher powers of $(v+\frac{1}{2})$. Such additional terms make a negligible contribution to the energies of lower vibrational levels, but can become very significant near the dissociation limit. Thus, the extrapolated values of D_e given in Table 8 are probably accurate only as to order of magnitude.

TABLE 8.

MEASURED VIBRATIONAL CONSTANTS OF CCl

Upper $^2\Delta$ State:

$\omega_e' = 860$ cm.$^{-1}$

$\omega_e x_e' = 7.5$ cm.$^{-1}$

$D_e' = 24,7000$ cm.$^{-1}$

Lower $^2\Pi$ State:

$\omega_{e''} = 875.1$ cm.$^{-1}$

$\omega_e x_e'' = 7.0$ cm.$^{-1}$

$D_e'' > 27,300$ cm.$^{-1}$

CHAPTER 10

DISCUSSION OF RESULTS OF THE CCl ANALYSES

The $^2\Pi$ lower state of the observed transition is almost certain to be the ground state of CCl, arising from the electron configuration: $\ldots (\pi)^4 (\sigma)^2 (\pi)$. The bond length of 1.65 A° in this state lies between the approximate values of 1.72 and 1.63 A° for C-Cl bonds adjacent to double and triple bonds respectively.[59] Similarly, Andrews and Barrow[55] found that the ground state internuclear distance for the CF radical is 1.27 A° , slightly less than the 1.32 A° found in CF groups adjacent to a double bond. The ground-state dissociation energy, D_0'', of CCl is 3.34 e.V.* As expected, it is less than the CF value of 4.96 e.V.

The splitting between the multiplet components of a case (a) state is expected to increase with the number of electrons, as does the analagous splitting of atomic multiplets. The doublet separation of the $^2\Pi$ lower state of CCl is 133.57 cm.$^{-1}$ NO and SiF, which also have twenty-three electrons, have $^2\Pi$ lower states with similar doublet separations of 121 and 160 cm.$^{-1}$ respectively. The CCl doublet separation is larger than the 77 cm.$^{-1}$ of CF, and smaller than the 207 cm.$^{-1}$ of SiCl, which have fifteen and thirty-one electrons respectively.[47]

The difference in energy of the dissociation products of the two observed electronic states of CCl is

$$\Delta E = T_0' + D_0' - D_0'' = 4.5 + 3 - 3.34 = 4 \text{ e.V.} \qquad (23)$$

*D_0 is the dissociation energy measured from the v = 0 vibrational level, and is slightly less than D_e, as defined in Chapter 9.

Most probably, the lower-state dissociation products of CCl are the normal C (^3P) and halogen (^2P) atoms, as was assumed by Andrews and Barrow[55] for CF. The upper $^2\Delta$ state of CCl can correlate with either: (i), the same normal atomic states, C (^3P) and Cl (^2P), as in the lower state; (ii), the states C ($2p\,^1D_2$) and Cl (^2P); or, (iii), a large number of excited states of both the carbon and chlorine atoms, or their ions C^+ and Cl^-. The ΔE values required by the first and second possibilities are 0 and 1.2 e.V. respectively. The possibilities (iii) require a ΔE value of 7 e.V. or more.[60] Although the D_0 values given in equation (22) are the results of drastic extrapolations, it is unlikely that they are so inaccurate that the true ΔE value is 0 e.V., or greater than 7 e.V. The upper-state dissociation products (ii) are thus the most likely.

The electron configuration . . . $(\pi)^4 (\sigma) (\pi)^2$ is a reasonable one for the $^2\Delta$ upper state of CCl. Mulliken[49] has predicted that the $^2\Delta$ state arising from this configuration has a narrow doublet separation, as was observed. The configuration . . . $(\pi)^4 (\sigma)^2 (\delta)$ is unlikely. One of the dissociation products of the molecular state arising from this configuration must be an atom with a d electron, and the dissociation products of lowest energy which meet this condition are C ($3d\,^1D_2$) and Cl (^2P), requiring a ΔE value of 9.7 e.V.

Finally, both the internuclear distance and the vibrational frequency in the upper state of CCl are smaller than the same quantities in the lower state, in apparent violation of the empirical rule,[47]

$$r_e^2 \omega_e \approx \text{a constant for a given molecule.} \qquad (24)$$

The product above, however, is expected to be constant only within ± 5%.

The products obtained for the two observed states of CCl differ by 4.5%. Eyster[54] specifically mentions having obtained similarly poor agreement in applying equation (24) to doublet states of the SiF molecule.

APPENDICES

I. DERIVATION OF ROTATIONAL ENERGY EXPRESSIONS FROM THE GENERAL HILL AND VAN VLECK EXPRESSION

The general Hill and Van Vleck expression for the rotational energy levels of a doublet state with coupling intermediate to cases (a) and (b) is given in Chapter 7 and is written below in a modified form.

$$\begin{Bmatrix} F_1(J) \\ F_2(J) \end{Bmatrix} = B_v \left[(J+\tfrac{1}{2})^2 - \Lambda^2 \mp \sqrt{(J+\tfrac{1}{2})^2 - \Lambda^2 + (Y-2)^2 \Lambda^2/4} \right] \quad (25)$$

Centrifugal stretching terms have been neglected. The constant D_v is given approximately[47] by $4B_v^3/\omega^2$, where ω is the vibrational frequency. Approximate values of $B_v = 0.7$ cm.$^{-1}$ and $\omega = 860$ cm.$^{-1}$ in both states may be obtained respectively from the spacing of rotational lines, and from the separation of the sequences. Thus, $D_v = 2 \times 10^{-6}$ cm.$^{-1}$, and the centrifugal stretching term for $J = 36.5$, the highest J value used in the analysis, is $D_v J^4 = 3.6$ cm.$^{-1}$ This is a significant contribution to the energy; however, the largest centrifugal stretching term appearing in the combination differences is $D_v J^3 = 0.1$ cm.$^{-1}$, and the largest such term appearing in the formulae for the branches is $(D_v' - D_v'')J^4$ which is even smaller. Since the measurement of the frequencies of the lines was accurate to only 0.15 cm.$^{-1}$, the centrifugal stretching terms were ignored.

For case (a) conditions it is assumed that $\left[(Y-2)^2\Lambda^2/4\right]$ $\gg\left[(J+\frac{1}{2})^2-\Lambda^2\right]$, and the square root may be expanded as follows:

$$(Y-2)\Lambda/2\left[1+4\left(\frac{(J+\frac{1}{2})^2-\Lambda^2}{(Y-2)^2\Lambda^2}\right)\right]^{\frac{1}{2}} = \tfrac{1}{2}Y - \Lambda \qquad (26)$$
$$+\frac{J(J+1)+(\frac{1}{4}-\Lambda^2)}{(Y-2)\Lambda} - \frac{\left[(J+\frac{1}{2})^2-\Lambda^2\right]^2}{(Y-2)^3\Lambda^3}+\ldots$$

The energy levels may then be written

$$\left\{\begin{matrix}F_1(J)\\F_2(J)\end{matrix}\right\} = B_v\left[\tfrac{1}{4}-(\Lambda\pm\tfrac{1}{2})^2\right]\mp\tfrac{1}{2}A\Lambda+\left\{\begin{matrix}(B_{eff})_1\\(B_{eff})_2\end{matrix}\right\}J(J+1)$$
$$\mp B_v\left[\frac{\frac{1}{4}-\Lambda^2}{(Y-2)\Lambda}-\frac{(J+\frac{1}{2})^2-\Lambda^2)^2}{(Y-2)^3\Lambda^3}+\ldots\right] \qquad (27)$$

where $\left\{\begin{matrix}(B_{eff})_1\\(B_{eff})_2\end{matrix}\right\} = B_v\left[1\mp1/(Y-2)\right]$. If it is assumed that the final term in square brackets in (27) and the difference between the two effective rotational constants, $(B_{eff})_i$, are negligible, this expression reduces to equation (5) of Chapter 7, which was derived directly from case (a) assumptions. The term $\frac{1}{2}B_v$ in equation (27) does not appear in equation (5), but it may be considered as part of the vibronic energy.[49] The term $B_v(\Lambda\pm\frac{1}{2})^2$ above corresponds to $B_v\Omega^2$ in equation (5).

Equation (27) may be used to represent the energy of the $^2\Pi_{reg}$ case (a) lower state of OCl if the effective rotational constants are used, and if the final term in square brackets is ignored. The observed separation of the two sub-bands indicates an approximate value of $1.40\pm.10$ cm.$^{-1}$ for the quantity $B_v(Y-2)$ in the lower state. This value, and the approximate value quoted above for B_v, may be used to show that the final

term in equation (27) does not exceed $\mp$ 0.05 cm.$^{-1}$ for $J \leq 36.5$. It is convenient to write the energies of the rotational levels of the $^2\Pi$ state as follows:

$$(^2\Pi_{\frac{1}{2}} \text{ component}): \quad F_1(J) = (B_{eff})_1 \, J(J+1) \qquad (28)$$

$$(^2\Pi 3/2 \text{ component}): \quad F_2(J) = B_v(Y-2) + (B_{eff})_2 J(J+1)$$

All terms independent of J and of Σ have been considered part of the vibronic energy. Since the $^2\Pi_{\frac{1}{2}}$ (v = 0) state is the lowest observed vibronic state of CCl, its energy is taken as zero.

For case (b) conditions it is assumed that $(J+\frac{1}{2})^2 \gg \alpha$, where $\alpha = Y(Y-4)\Lambda^2/4$. The square root in the Hill and Van Vleck expression can thus be expanded

$$(J+\tfrac{1}{2})\left[1 + \alpha/(J \ \tfrac{1}{2})^2\right]^{\frac{1}{2}} = (J+\tfrac{1}{2}) + \alpha/2(J+\tfrac{1}{2}) + \ . \ . \ . (29)$$

If the spin splitting described in Chapter 7 is included, and the appropriate substitutions of K for J are made (i.e. $J = K + \frac{1}{2}$ for F_1 levels and $J = K - \frac{1}{2}$ for F_2 levels), the case (b) energy levels become

$$\begin{Bmatrix} F_1(K) \\ F_2(K) \end{Bmatrix} = B_v\left[K(K+1) - \Lambda^2\right] - Y/4 + \begin{Bmatrix} -H(J=K+\frac{1}{2}) \\ +H(J=K-\frac{1}{2}) \end{Bmatrix} \qquad (30)$$

$$\text{where } H(J) = \left[-\tfrac{1}{2}\gamma(J+1) + B_v\alpha/2(J+\tfrac{1}{2}) + \ . \ . \ .\right]$$

$$\simeq B_v\left[\sqrt{(J+\tfrac{1}{2})^2+\alpha} \ -(J+\tfrac{1}{2})\right] - \tfrac{1}{2}\gamma(J+1).$$

If the terms H(J) and $(-\frac{1}{2}\gamma)$ are sufficiently small to be neglected, equation (30) is identical to equation (6) of

Chapter 7 which was derived directly from case (b) assumptions.

If all terms independent of J (or of K) and of the orientation of the spin are considered part of the vibronic energy F_0, referred to the same zero as in equation (27), the case (b) energy levels are conveniently written in terms of J as follows:

$$\begin{aligned} F_1(J) &= F_0 + B_v(J-\tfrac{1}{2})(J+\tfrac{1}{2}) - H(J) \\ F_2(J) &= F_0 + B_v(J+\tfrac{1}{2})(J+3/2) + H(J) \end{aligned} \qquad (31)$$

II. FORMULAE FOR THE FREQUENCIES OF THE LINES IN A $^2\Delta$ CASE (b) - $^2\Pi_{reg}$ CASE (a) TRANSITION

Neglecting the effects of Λ-type doubling, twelve branches are expected for a transition of this type. As shown in Fig. 15 of Chapter 7, each branch is defined by the ΔJ and ΔK values of the corresponding transition. The symbols P, Q, and R designate ΔJ values of -1, 0, and 1 respectively. Except for transitions involving the $J = 1.5$ level of the $^2\Delta$ upper state, it is possible to write the frequencies of the lines of each branch in the following form, using the energy expressions given by equations (28) and (31) of Appendix I:

$$\nu = [F_i'(\text{upper state } J \text{ value}) - F_i''(\text{lower state } J \text{ value})] \qquad (32)$$

where $i = 1$ or 2, and where the superscripts ' and " designate upper and lower-state quantities respectively. The numerical subscripts in the branch symbols give the value of i. For example, the symbol R_2 (or R_1) indicates that $i = 2$ (or 1) in both states. If two numbers appear, as in R_{21}, they indicate respectively the value of i in the upper and in the lower state.

The twelve branches are listed in Table 9, along with the ΔK and ΔJ values which define them, and with formulae for the frequencies of their lines. The origins of the two subbands, $^2\Delta - ^2\Pi_{\frac{1}{2}}$ and $^2\Delta - ^2\Pi_{3/2}$, are $\nu_0(1) = F_0'$ and $\nu_0(2) = F_0' - B_v''(Y''-2)$ respectively. The lines in each branch are designated by the J value of the lower-state level of the corresponding transition. The J value of the first line of

TABLE 9.

FORMULAE FOR THE BRANCHES OF A $^2\Delta$ CASE (b) - $^2\Pi_{reg}$ CASE (a) TRANSITION

BRANCHES				FORMULAE
ΔJ	$^2\Delta - {}^2\Pi_{1/2}$ (i = 1)	ΔK	$^2\Delta - {}^2\Pi_{3/2}$ (i = 2) ΔK	
-1	P_1 (3.5)	-1	P_{12} (3.5) -2	$\nu = F_1'(J-1) - F_i''(J) = [\nu_0(i) + \frac{3}{4}B_v'] - [2B_v' + (B_{eff})_i''] J + \Delta B_i J^2 - H(J-1)$.
-1	P_{21} (2.5)	0	P_2 (2.5) -1	$\nu = F_2'(J-1) - F_i''(J) = [\nu_0(i) - \frac{1}{4}B_v'] - (B_{eff})_i'' J + \Delta B_i J^2 + H(J-1)$.
0	Q_1 (2.5)	0	Q_{12} (2.5) -1	$\nu = F_1'(J) - F_i''(J) = [\nu_0(i) - \frac{1}{4}B_v'] - (B_{eff})_i'' J + \Delta B_i J^2 - H(J)$.

0	Q_{21} (1.5)	1	Q_2 (1.5)	0	$\nu = F_2'(J) - F_i''(J) = [\nu_0(i) + \frac{3}{4}B_v'] + [2B_v' - (B_{eff})_i''] J + \Delta B_i J^2 + H(J).$
1	R_1 (1.5)	1	R_{12} (1.5)	0	$\nu = F_1'(J+1) - F_i''(J) = [\nu_0(i) + \frac{3}{4}B_v'] + [2B_v' - (B_{eff})_i''] J + \Delta B_i J^2 - H(J+1).$
1	R_{21} (0.5)	2	R_2 (1.5)	1	$\nu = F_2'(J+1) - F_i''(J) = [\nu_0(i) + 15/4\ B_v'] + [4B_v' - (B_{eff})_i''] J + \Delta B_i J^2 + H(J+1).$

$$\Delta B_i = B_v' - (B_{eff})_i''$$

each branch is given in brackets below the branch symbol. The branches are listed in pairs, one from each sub-band, and the correct frequencies are obtained by taking the value indicated for the symbol i.

The $^2\Delta(J=1.5)$ level has the energy $F_1'(1.5)$ for $Y'>2$, and $F_2'(1.5)$ for $Y'<2$. Thus, the general expression of equation (32), and hence the formulae of Table 9, cannot be used for lines involving this anomalous level. The lines which must be treated separately are $P_{21}(2.5)$, $P_2(2.5)$, $Q_{21}(1.5)$, $Q_2(1.5)$, and $R_{21}(0.5)$. For $Y'<2$, the formulae of Table 9 may be used for these five lines; for $Y'>2$, the correct formulae are obtained from those of Table 9 by changing the sign of H(J).

Except for the term H(J), which accounts for a tendency towards case (a) in the case (b) upper state, the formulae for the branches are parabolic. If the tendency towards case (a) is large, the deviation from a parabolic form is quite marked at low J values, as illustrated in Fig. 16(b) of Chapter 7.

The parabolic or near-parabolic form of the branches indicates that some of them will form heads. Which ones are head-forming depends on the sign of ΔB_i. The Fortrat diagrams in Fig. 16 of Chapter 7 correspond to $\Delta B_i > 0$. This in turn implies that the internuclear distance is greater in the lower than in the upper state. Bands in which heads are formed on the low frequency side of the band origins are described as being "degraded to higher frequencies" or "violet-degraded".

III. FREQUENCIES AND ROTATIONAL ASSIGNMENTS OF THE OBSERVED LINES IN THE 2780 A° BAND OF CCl

The following table lists the frequencies and rotational assignments of the observed lines in the 2780 A° band of CCl. If fine structure appears in a given line, the frequency quoted is the mean of the frequencies of the fine-structure components.

The numbering of the lines of the P_{12}, Q_2, R_2, P_1, R_1, and R_{21} branches is discussed in Chapter 8. Observed lines of other branches were identified by a calculation of their frequencies from the formulae of Appendix II and the data of Table 6.

TABLE 10

VACUUM WAVENUMBERS AND ROTATIONAL ASSIGNMENTS FOR THE 2780 A° BAND OF CCl.

	$(^2\Delta - ^2\Pi_{\frac{1}{2}})$			$(^2\Delta - ^2\Pi_{3/2})$				
J	R_{21}	R_1	P_1	R_2	R_{12}	Q_2	P_2	P_{12}
1.5		35998.93		35876.64	35865.60	35872.96		
2.5		36000.10		878.66	866.57	873.34	35869.63	
3.5		001.29		880.60	867.69	873.80	868.75	
4.5		002.43	35988.98	882.45	868.75	874.38	867.41	
5.5		003.56	987.46	884.36	869.63	874.90	866.57	
6.5		004.71	985.92	886.38	870.63	875.36	865.71	35851.97
7.5		005.59	984.31	888.43	872.04	875.95	864.88	850.25
8.5		007.01	982.67	890.49		876.64	864.17	848.49
9.5		008.12	981.04	892.79		877.36	863.54	846.81
10.5		009.30	979.45	894.97		878.13	862.73	844.94
11.5		010.50	977.79	897.20		878.94		843.52
12.5		011.68	976.28	899.41		879.75		841.44

13.5		36012.80	35974.75	35901.70	35880.60	35839.76
14.5		014.31	973.09	904.02	881.52	837.97
15.5		015.48	971.83	906.35	882.45	836.22
16.5	36044.36	016.69	970.09	908.83	883.37	834.50
17.5	046.65	017.99	968.63	911.10	884.36	832.81
18.5	049.52	019.47	967.17	913.49	885.56	831.09
19.5	052.24	021.10	965.72	915.92	886.68	829.40
20.5	054.92	022.23	964.34	918.38	887.40	827.73
21.5	057.67	023.65	962.98	920.84	888.43	826.09
22.5	060.48	025.10	961.62	923.30	889.54	824.45
23.5	063.29	026.63	960.33	925.82	890.59	822.83
24.5	066.09	028.10	959.06	928.35	891.75	821.23
25.5	069.01	029.72	957.63	930.89	892.76	819.61
26.5	071.92	031.27	956.59	933.57	894.07	818.05
27.5	074.79	032.68		936.05	895.23	816.52

28.5	36077.82	36034.28	35938.59	35896.39	35814.58
29.5	080.47	035.91	941.24	897.64	813.73
30.5	083.83	037.54	943.88	898.86	811.98
31.5	086.92	039.16	946.56	900.29	810.51
32.5	089.98	040.86	949.19	901.41	809.04
33.5	093.10	042.62	951.89	902.71	807.64
34.5	096.26		954.40	904.02	806.20
35.5	099.49			905.52	804.82
36.5	102.63			906.66	803.40
37.5					802.08
38.5					800.75
39.5					799.44
40.5					798.08
41.5					796.82
42.5					795.54

BIBLIOGRAPHY

1. D. A. Ramsay, Adv. in Spec., 1 1 (1959).

2. P. Venkateswarlu, Phys. Rev., 77 676 (1950).

3. T. E. Khalafawi and A. Johannin-Gilles, Compt. Rendus, Acad. Sci. Paris, 242 1716 (1956).

4. R. K. Laird, E. B. Andrews, and R. F. Barrow, Trans. Faraday Soc., 46 803 (1950).

5. G. Herzberg, Proc. Chem. Soc., 1959 116.

6. A. D. Walsh, J. Chem. Soc., 1953 2230,2260.

7. R. G. W. Norrish and G. Porter, Nature, 164 658 (1949).

8. G. Herzberg and D. A. Ramsay, Disc. Faraday Soc., 9 80 (1950).

9. N. Davidson, R. Marshall, A. E. Larsh, and T. J. Carrington, J. Chem. Phys., 19 1311 (1951).

10. J. U. White, J. Opt. Soc. Am., 32 285 (1942).

11. J. L. Margrave and K. Wieland, J. Chem. Phys., 21 1552 (1953).

12. K. T. Compton and I. Langmuir, Rev. Mod. Phys., 2 123,(1930), 3 191 (1931).

13. H. Schuler, Spec. Acta 4 85 (1950); Z. fur Nat. A, 5 (1950).

14. J. H. Callomon, Can. J. Phys., 34 1046 (1956).

15. L. Goldstein, Adv. in Electronics and Electron Physics, 7 399 (1955).

16. R. L. McCarthy, J. Chem. Phys., 22 1360 (1954).

17. J. P. Simons and A. J. Yarwood, Nature, 187 316 (1960).

18. P. J. Dyne, Can. J. Phys., 31 453 (1953).

19. A. E. Douglas, private communication.

20. G. Herzberg and J. Shoosmith, Nature 183 1801 (1959).

21. J. W. C. Johns, G. W. Chantry, and R. F. Barrow, Trans. Faraday Soc., 54 1589 (1958).

22. Ellis and Wells. The Chemical Action of Ultraviolet Rays. Heyroth Publishing Co.,New York 1925.

23. R. F. Barrow, Nature, 165 890 (1950); Proc. Phys. Soc. A, 64 481 (1951).

24. Y. Y. Kuzyakov and V. M. Tatevskyi, Nauchnye Vysshei Shkoly. Khimiia i Khimicheskaii Teknologiia, 2 233,(1959).

25. Y. Y. Kuzyakov and V. M. Tatevskyi, ibid., 2 237 (1959).

26. R. F. Barrow, Proc. Phys. Soc. A, 67 186 (1954).

27. W. Jevons, Proc. Roy. Soc. A, 106 174 (1924).

28. R. K. Asundi and S. M. Karim, Proc. Ind. Acad. Sci. A, 6 328 (1937).

29. T. Horie, Proc. Phys. Math. Soc. Japan, 21 143 (1939).

30. P. Venkateswarlu, Phys. Rev., 77 79 (1950).

31. Y. Y. Kuzyakov and V. M. Tatevskyi, Optics and Spec., 7 300 (1959).

32. W. H. B. Cameron and A. Elliott, Proc. Roy. Soc. A, 158 681 (1937), 164 531 (1938), 169 463 (1939).

33. R. K. Asundi, N. L. Singh, and J. P. Mishra, Current Sci., 12 204 (1943).

34. H. G. Gale and G. S. Monk, Phys. Rev.,29 211 (1923).

35. P. Venkateswarlu, Proc. Ind. Acad. Sci. A, 25 138 (1947).

36. R. W. B. Pearse and A. G. Gaydon, The Identification of Molecular Spectra. Chapman and Hall, London 1950.

37. Handbook of Physics and Chemistry, 38th Edition, Chemical Rubber Publishing Co., Cleveland, Ohio 1956.

38. G. Herzberg. Atomic Spectra and Atomic Structure. Dover, New York 1944.

39. P. B. V. Haranath and P. T. Rao, J. Mol. Spec., 2 428 (1958); Ind. J. Phys., 29 205 (1955).

40. V. Kondratjew and A. Leipunsky, Trans. Faraday Soc., 25 736 (1929).

41. R. K. Asundi and R. Samuel, Proc. Ind. Acad. Sci. A, 3 346 (1936).

42. G. Pannetier and P. Lafitte, Compt. Rendus, Acad. Sci. Paris, 226 72 (1948).

43. G. W. King, J. Sci. Instr., 35 11 (1958).

44. G. R. Harrison. MIT Wavelength Tables. John Wiley and Sons, Inc., New York 1939.

45. B. Edlen, J. Opt. Soc. Am., 43 339 (1953).

46. J. H. Callomon, Proc. Roy. Soc. A, 244 220 (1958).

47. G. Herzberg. Spectra of Diatomic Molecules. D. Van Nostrand Co., Ltd., Princeton, N.J. 1950.

48. R. C. Johnson. Spectra. Methuen and Co., Ltd., London 1941.

49. R. S. Mulliken, Rev. Mod. Phys., 2 60 (1930), 3 89 (1931), 4 1 (1932).

50. R. S. Mulliken and A. Christy, Phys. Rev., 38 87 (1931).

51. E. L. Hill and J. H. Van Vleck, Phys. Rev., 32 250 (1928).

52. J. H. Van Vleck, Phys. Rev., 33 467 (1929).

53. C. H. Townes and A. L. Schawlow. Microwave Spectroscopy. McGraw Hill, New York 1955.

54. E. H. Eyster, Phys. Rev., 51 1078 (1937).

55. E. B. Andrews and R. F. Barrow, Proc. Phys. Soc. A, 64 481 (1951).

56. I. E. Ovcharenko, L. N. Tunitskii, and V. I. Yakatin, Optics and Spec., 8 393 (1960).

57. R. Schmid, Z. Physik, 64 84, 64 279 (1930).

58. R. T. Birge, Rev. Mod. Phys., 19 298 (1947).

59. H. J. M. Bowen, et al.Tables of Interatomic Distances and Configuration in Molecules and Ions. Special Publication No. 11, The Chemical Society, London 1958.

60. C. E. Moore, et al. Atomic Energy Levels. Circular of the National Bureau of Standards 467. U. S. Department of Commerce, 1949.

61. R. D. Gordon and G. W. King, Can. J. Phys., in press (1961).